Arabian Journal of Geosciences (2021) 14: 1341
https://doi.org/10.1007/s12517-021-07574-6

ORIGINAL PAPER

# Geochemical characteristics of carbonates and indicative significance of the sedimentary environment based on carbon-oxygen isotopes, trace elements and rare earth elements: case study of the Lower Paleozoic carbonates in the Gucheng area, Tarim Basin, China

Xiaoxiao Zhou[1,2] · Xiuxiang Lü[3] · Ce Liu[1]

Received: 19 January 2021 / Accepted: 10 June 2021 / Published online: 7 July 2021


## Abstract

Carbonate rocks are important targets of hydrocarbon exploration in the Gucheng area, Tarim Basin. In this study, the thin sections, carbon and oxygen isotopes, trace elements and rare earth elements of 25 carbonate samples from the Upper Cambrian and the Ordovician are conducted to research the original sedimentary environment of these carbonate rocks. The carbonate rocks have undergone high-temperature hydrothermal activity due to the movement of magmatic water in the Permian based on carbon and oxygen isotope and $Eu_{anom}$ data. The Upper Cambrian and Ordovician are divided into five third-order sequences based on carbon isotopes and natural gamma-ray spectral logging combined with previous researches. The SQ1~SQ3 in the Upper Cambrian and Middle-Lower Ordovician predominant in sea-level decline cycle, whereas the SQ4 and SQ5 in the Middle-Upper Ordovician are dominated by sea-level rise cycle. $Ce_{anom}$ and Z values are suitable to analyze the redox environment and paleosalinity quantitatively, which suggests an oxidizing and marine origin in this area. The dolomites are formed in a paleoenvironment with a higher salinity, a stronger oxidation and a lower falling sea level than that of the limestones.

**Keyword** Gucheng area · Lower Paleozoic · Paleoenvironment · Carbon and oxygen isotopes · Trace elements Rare earth elements

## Introduction

Primitive geochemical informations, such as carbon-oxygen isotopes, trace element, and rare earth elements (REEs), are kept in deposit sediments. These elements and stable isotopes contain abundant informations about paleoclimate, paleosalinity, and paleodepth. Therefore, the contents, ratios and relative correlations of these geochemical parameters can be applied to reconstruct the original sedimentary environment. These indicators have been widely used for mudstone and shale (Mongenot et al. 1996; Yu et al. 2009; Cao et al. 2012; Wang et al. 2014a; Akinlua et al. 2015, 2016). Because the enrichment mechanisms of elements and stable isotopes in various sedimentary rocks are the same, many scholars also study the marine sedimentary paleoenvironment by stable isotopes and elements (Wignall and Twitchett 1996; Schroeder and Grotzinger 2007; Wignall et al. 2007; Frimmel 2009; Xu et al. 2009; Meyer et al. 2012; Chen et al. 2013; Wei et al. 2015).

In the Gucheng area, Tarim Basin, oil and gas exploration shows that hydrocarbons mainly accumulate in the Ordovician. The sedimentary facies, sequence, reservoir characteristics, and dolomite genesis of the Lower Paleozoic in the Gucheng area have been researched by many scholars (Zhao et al. 2009; Liu et al. 2012; Tang et al. 2013; Wang et al. 2014b; Wang et al. 2015; Liu et al. 2017). However, those studies have focused more on petrological, paleontological,

Responsible Editor: Attila Ciner

✉ Xiaoxiao Zhou
zxaBMJD199@163.com

[1] Dongxin Oil Production Plant, Dongying 257000, China

[2] Working Stations for Postdoctors of Shengli Oilfield, Dongying 257000, China

[3] SINOPEC (China Petrochemical Corporation), Shengli oilfield company, Dongying 257000, China

and seismic reflection characteristics. Few scholars have reconstructed the sedimentary paleoenvironment based on geochemical parameters such as carbon and oxygen isotopes, REEs, and trace elements of carbonate rocks. In this study, the applicability of these geochemical indicators about paleoenvironment is discussed. Moreover, the sedimentary paleoenvironment and evolution process of carbonate rocks in the Ordovician and Upper Cambrian are researched based on appropriate geochemical indicators. The research results provide a comprehensive understanding of the geological environment of the Lower Paleozoic carbonate rocks in the Gucheng area and perhaps they are helpful for the study of the Lower Paleozoic carbonate reservoir.

## Geologic background

The Tarim Basin is a large superimposed basin composed of marine craton basin in the Paleozoic and continental foreland basin in the Meso-Cenozoic (Jia 1999) with an area of $5.6\times10^{-5}$ km$^2$. The basin is controlled by multistage tectonic movement and contains 9 first-order structural units, i.e., four uplifts and five depressions, each of which includes various numbers of second-order units (Fig. 1). Carbonate rocks are deposited in the Lower Paleozoic, including the Cambrian and Ordovician rocks in the Gucheng area. According to Cao et al. (2019), the Cambrian from bottom to top contains the Yurtus, Xiaoerbulak, and Wusongger Formations in the Lower Cambrian, Shaylik and Awatag Formations in the Middle Cambrian, and the Lower Qiulitag Formation in the Upper Cambrian. The Ordovician rocks from bottom to top include the Penglaiba Formation, the lower of Yingshan (Ying 4~Ying 3 Members), the upper of Yingshan (Ying 2~Ying 1 Members) and the Yijianfang Formation in the Middle-Lower Ordovician, and the Tumuxiuk and Querquek Formations in the Upper Ordovician (Fig. 2).

The Gucheng area has experienced 4 main stages of structural evolution. (1) In the tectonic extension stage from the Cambrian to Middle Ordovician, the Gucheng area, Tazhong, Shuntuoguole, and Tabei areas were a unified carbonate platform (Zhang et al. 2015). (2) In the late stage of Middle Ordovician, the Tazhong area suffered a strong compression and denudation, resulting in a partial absence of the Upper Ordovician in the principal part of the Tazhong area (Yang et al. 2000; Zhang et al. 2004). Because the Gucheng area was located at a structural slope, the Yijianfang Formation with slope facies was deposited in this area (Cai et al. 2006). (3) In the early stage of the Late Ordovician, the tectonic stress of the basin changed from tension to compression (Zhang et al. 2007). As a result, the facies rapidly changed into shelf basin facies, and clastic rocks with thicknesse greater than 4000 m were deposited with increasing sea level. (4) In the Middle-Late Ordovician, the nose structure of the Gucheng area gradually formed, and a large number of SE–NW direction faults were developed, which controlled the later horst-graben tectonic framework (Li et al. 2018; Tang et al. 2014).

## Samples and analytical methods

All these core samples in this study are from GC7 Well. Fresh samples are taken to avoid calcite veins, pyrite crystals, and

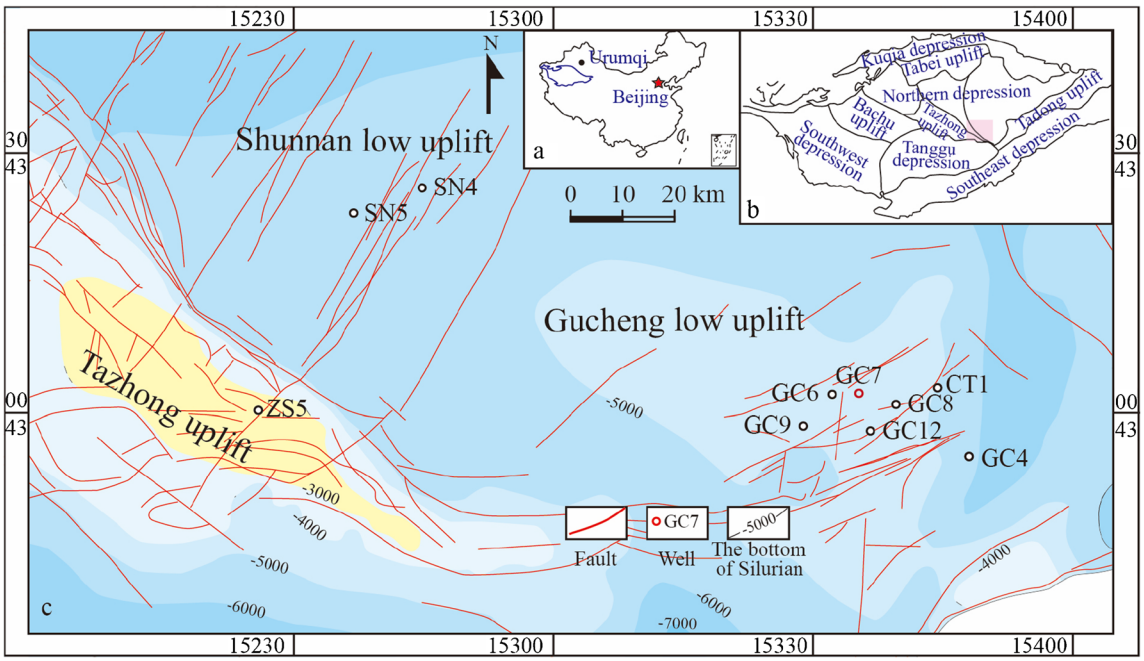


**Fig. 1.** Division of tectonic units of the Gucheng area (GC7 Well is a systematic sampling well)

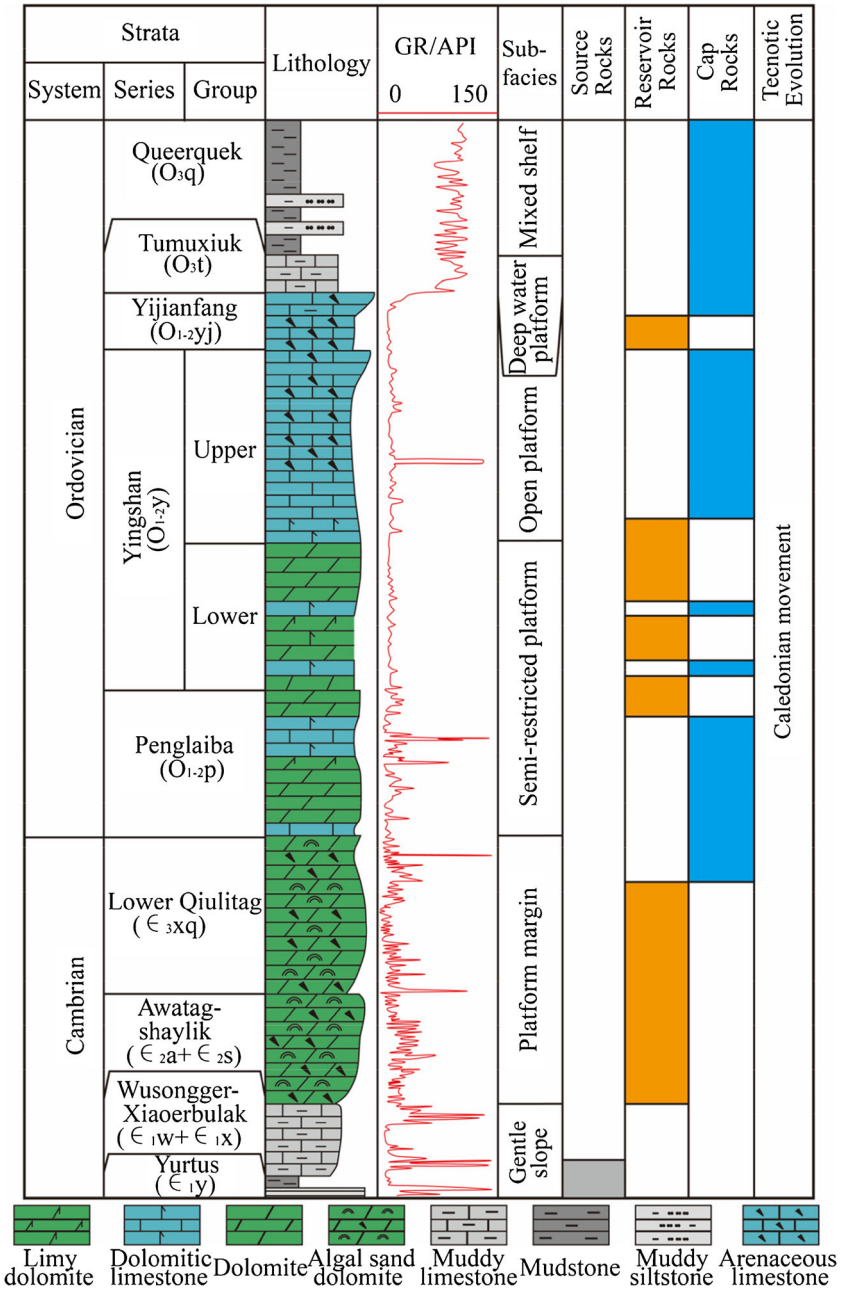


**Fig. 2.** Composite stratigraphic columnar section of the Lower Paleozoic in the Gucheng area (Modified by Cao et al. 2019)

recrystallization. To avoid the influence of diagenesis, all samples are first ground into thin slices, and the mineral composition and structural characteristics are observed in detail under a microscope. Then, limestone, dolomite, marlstone, and some transitional lithologies with micritic textures are selected, and the sampling range is narrowed as much as possible. Finally, 25 samples are taken for analysis, which include 7 samples from the Lower Qiulitag Formation of the Upper Cambrian and 18 samples from the Ordovician, containing 4 samples from the Penglaiba Formation, 3 samples from the Ying 4 Member, 8 samples from the Ying 3 Member, and 3 sample from the Ying 1 Member, the Yijianfang Formation, and the Tumuxiuk Formation, respectively. These samples are analyzed with carbon and oxygen isotopes, REEs, and trace elements. Experimental data are listed in Table 1 and Table 2. The related experimental methods are listed as follows.

## Thin section analysis

Conventional thin sections are ground at the China University of Petroleum (Beijing). These thin sections are identified at 10×5 magnification with an Imager A2m polarized fluorescence microscope made by Carl Zeiss corporation in Germany according to the People Republic of China petroleum natural gas profession standard (SY/T 6103-2004 and SY/T5368-2016).

**Table 1** Distribution of carbon and oxygen isotopes and REEs of carbonate rocks in the Paleozoic of GC7 Well. Note: $Ce_{anom} = Ce/Ce^{*} = (3Ce_{PASS}/(2La_{PASS} + Pr_{PASS}))$ (McLennan 1989); PASS stands for the ratio after PASS standardization; $Eu_{anom}$ ($Eu/Eu^{*}_{PAAS}$) = $Eu_{PAAS}/(Sm_{PAAS} \times Gd_{PAAS})^{1/2}$ (Taylor and Mclennan 1985). In this study, Gd is replaced by Tb in the formula of $Eu_{anom}$

| No. | Depth (m) | Strata | Lithology | $\delta^{13}$Ccarb (‰, PDB) | $\delta^{18}$Ocarb (‰, PDB) | Z | Rare-earth element (ppm) | | | | | | | | | | | | | $Eu_{anom}$ | $Ce_{anom}$ |
|---|---|---|---|---|---|---|---|---|---|---|---|---|---|---|---|---|---|---|---|---|---|
| | | | | | | | La | Ce | Pr | Nd | Sm | Eu | Tb | Dy | Ho | Er | Tm | Yb | Lu | | |
| 1 | 5622.0 | $O_3t$ | Micritic bioclastic limestone | 1.09 | -10.84 | 124.13 | 4.66 | 9.42 | 1.60 | 12.99 | 1.14 | 0.25 | 0.19 | 1.03 | 0.20 | 0.55 | 0.09 | 0.61 | 0.10 | 1.03 | 0.57 |
| 2 | 5689.0 | $O_{1\text{-}2}yj$ | Sparite calcarenites | -0.34 | -6.48 | 123.38 | 0.10 | 0.21 | 0.04 | 0.31 | 0.03 | 0.01 | 0.00 | 0.02 | 0.01 | 0.01 | 0.00 | 0.02 | 0.00 | 1.21 | 0.53 |
| 3 | 5731.0 | $O_{1\text{-}2}y1$ | Sparite calcarenites | -1.72 | -6.86 | 120.36 | 0.20 | 0.40 | 0.07 | 0.59 | 0.05 | 0.01 | 0.01 | 0.04 | 0.01 | 0.02 | 0.00 | 0.02 | 0.00 | 1.24 | 0.53 |
| 4 | 6023.0 | $O_{1\text{-}2}y3$ | Sparite calcarenite | -1.96 | -7.92 | 119.34 | 0.30 | 0.57 | 0.10 | 0.78 | 0.07 | 0.02 | 0.01 | 0.06 | 0.01 | 0.03 | 0.01 | 0.03 | 0.01 | 1.16 | 0.56 |
| 5 | 6110.0 | $O_{1\text{-}2}y3$ | Fine crystalline | -2.15 | -6.5 | 119.66 | 0.57 | 1.25 | 0.22 | 1.92 | 0.16 | 0.03 | 0.03 | 0.14 | 0.03 | 0.08 | 0.01 | 0.08 | 0.01 | 0.98 | 0.54 |
| 6 | 6140.0 | $O_{1\text{-}2}y3$ | Sparite calcarenite | -0.74 | -9.06 | 121.27 | 0.29 | 0.54 | 0.09 | 0.72 | 0.06 | 0.01 | 0.01 | 0.05 | 0.01 | 0.03 | 0.00 | 0.03 | 0.00 | 1.15 | 0.56 |
| 7 | 6161.0 | $O_{1\text{-}2}y3$ | Fine crystalline dolostone | -0.83 | -8.93 | 121.15 | 0.44 | 0.90 | 0.17 | 1.56 | 0.13 | 0.03 | 0.02 | 0.13 | 0.02 | 0.07 | 0.01 | 0.08 | 0.01 | 0.97 | 0.49 |
| 8 | 6184.0 | $O_{1\text{-}2}y3$ | Sparite calcarenite | -1.1 | -11.12 | 119.51 | 0.40 | 0.78 | 0.13 | 1.11 | 0.10 | 0.02 | 0.01 | 0.08 | 0.01 | 0.04 | 0.01 | 0.04 | 0.01 | 1.15 | 0.55 |
| 9 | 6192.3 | $O_{1\text{-}2}y3$ | Mesocrystalline dolostone | -0.95 | -6.36 | 122.19 | 0.30 | 0.54 | 0.10 | 1.06 | 0.07 | 0.01 | 0.01 | 0.05 | 0.01 | 0.03 | 0.00 | 0.03 | 0.00 | 1.05 | 0.43 |
| 10 | 6230.0 | $O_{1\text{-}2}y3$ | Fine crystalline dolostone | -0.54 | -8.06 | 122.18 | 0.20 | 0.38 | 0.07 | 0.99 | 0.05 | 0.01 | 0.01 | 0.04 | 0.01 | 0.02 | 0.00 | 0.02 | 0.00 | 1.07 | 0.37 |
| 11 | 6241.0 | $O_{1\text{-}2}y3$ | Sparite calcarenite | -0.9 | -12.63 | 119.17 | 0.33 | 0.57 | 0.09 | 0.75 | 0.06 | 0.02 | 0.01 | 0.05 | 0.01 | 0.03 | 0.00 | 0.03 | 0.00 | 1.15 | 0.55 |
| 12 | 6316.5 | $O_{1\text{-}2}y4$ | Sparite calcarenite | 0.68 | -8.95 | 124.24 | 0.19 | 0.37 | 0.06 | 0.50 | 0.04 | 0.01 | 0.01 | 0.04 | 0.01 | 0.02 | 0.00 | 0.02 | 0.00 | 1.12 | 0.57 |
| 13 | 6337.0 | $O_{1\text{-}2}y4$ | Fine-medium crystalline dolostone | -0.24 | -7.63 | 123.01 | 0.54 | 1.00 | 0.16 | 1.39 | 0.11 | 0.02 | 0.02 | 0.09 | 0.02 | 0.04 | 0.01 | 0.04 | 0.01 | 1.09 | 0.55 |
| 14 | 6399.0 | $O_{1\text{-}2}y4$ | Fine-medium crystalline dolostone | -0.38 | -8.31 | 122.38 | 0.39 | 0.81 | 0.13 | 1.20 | 0.09 | 0.02 | 0.01 | 0.08 | 0.01 | 0.04 | 0.01 | 0.04 | 0.01 | 1.14 | 0.55 |
| 15 | 6429.5 | $O_{1\text{-}2}P$ | Fine-silty crystalline dolostone | -0.33 | -8.54 | 122.37 | 0.40 | 0.74 | 0.13 | 1.36 | 0.09 | 0.02 | 0.01 | 0.06 | 0.01 | 0.04 | 0.01 | 0.04 | 0.01 | 1.29 | 0.46 |
| 16 | 6499.0 | $O_{1\text{-}2}P$ | Silty crystalline dolostone | 0.58 | -5.99 | 125.50 | 0.88 | 1.59 | 0.29 | 2.43 | 0.20 | 0.05 | 0.03 | 0.15 | 0.03 | 0.08 | 0.01 | 0.09 | 0.01 | 1.13 | 0.51 |
| 17 | 6510.0 | $O_{1\text{-}2}P$ | Fine-silty crystal dolostone | -0.34 | -10.57 | 121.34 | 0.55 | 1.12 | 0.20 | 1.88 | 0.17 | 0.05 | 0.02 | 0.13 | 0.02 | 0.07 | 0.01 | 0.08 | 0.01 | 1.40 | 0.50 |
| 18 | 6520.0 | $O_{1\text{-}2}P$ | Fine crystalline dolostone | 0.78 | -9.51 | 124.16 | 0.18 | 0.35 | 0.06 | 0.77 | 0.05 | 0.01 | 0.01 | 0.04 | 0.01 | 0.02 | 0.00 | 0.02 | 0.00 | 1.35 | 0.42 |
| 19 | 6640.0 | $Є_3xq$ | Medium-coarse crystalline dolostone | -0.63 | -9.06 | 121.50 | 0.19 | 0.37 | 0.07 | 0.68 | 0.05 | 0.01 | 0.01 | 0.04 | 0.01 | 0.02 | 0.00 | 0.02 | 0.00 | 1.35 | 0.46 |
| 20 | 6643.2 | $Є_3xq$ | Coarse crystalline dolostone | -1.2 | -10.61 | 119.56 | 0.15 | 0.32 | 0.06 | 0.90 | 0.09 | 0.04 | 0.01 | 0.04 | 0.01 | 0.02 | 0.00 | 0.02 | 0.00 | 2.87 | 0.35 |
| 21 | 6643.5 | $Є_3xq$ | Coarse crystalline dolostone | -1.01 | -10.24 | 120.13 | 0.15 | 0.31 | 0.06 | 0.72 | 0.33 | 0.20 | 0.01 | 0.04 | 0.01 | 0.02 | 0.00 | 0.02 | 0.00 | 8.14 | 0.41 |
| 22 | 6679.0 | $Є_3xq$ | Medium-coarse crystalline dolostone | -0.98 | -10.15 | 120.24 | 0.43 | 0.69 | 0.12 | 1.01 | 0.09 | 0.08 | 0.01 | 0.07 | 0.01 | 0.04 | 0.00 | 0.04 | 0.01 | 4.65 | 0.50 |
| 23 | 6724.0 | $Є_3xq$ | Medium-coarse crystalline dolostone | -0.42 | -10.62 | 121.15 | 0.87 | 1.74 | 0.32 | 2.66 | 0.24 | 0.11 | 0.05 | 0.31 | 0.07 | 0.18 | 0.03 | 0.21 | 0.03 | 1.97 | 0.53 |
| 24 | 6750.0 | $Є_3xq$ | Sparite calcarenite | 0.12 | -12.53 | 121.31 | 0.40 | 0.75 | 0.12 | 0.97 | 0.08 | 0.02 | 0.01 | 0.07 | 0.01 | 0.04 | 0.01 | 0.03 | 0.01 | 1.35 | 0.57 |
| 25 | 6779.0 | $Є_3xq$ | Medium-coarse crystalline dolostone | -0.85 | -9.64 | 120.76 | 0.18 | 0.38 | 0.07 | 0.86 | 0.07 | 0.03 | 0.01 | 0.05 | 0.01 | 0.02 | 0.00 | 0.02 | 0.00 | 2.08 | 0.41 |

**Table 2** Trace elements of carbonate rocks in the Lower Paleozoic of GC7 Well

| No. | Depth (m) | Strata | Trace element (ppm) | | | | | | | | | | | | | | | | | | U/Th | Sr/Ba |
|---|---|---|---|---|---|---|---|---|---|---|---|---|---|---|---|---|---|---|---|---|---|---|
| | | | Ba | Cd | Cr | Cs | Hf | Li | Mn | Nb | Ni | Pb | Sr | Ta | Th | Ti | U | W | Y | Rb | Sc | | |
| 1 | 5622.0 | $O_3t$ | 30.58 | 0.01 | 6.42 | 0.68 | 0.62 | 3.32 | 1010.8 | 1.72 | 20.37 | 17.61 | 229.8 | 0.11 | 2.07 | 282.89 | 0.25 | 0.262 | 9.33 | 11.62 | 2.98 | 0.12 | 7.52 |
| 2 | 5689.0 | $O_{1\text{-}2}yj$ | 3.46 | 0.00 | 0.26 | 0.01 | 0.02 | 0.10 | 38.1 | 0.04 | 19.73 | 0.31 | 226.1 | 0.00 | 0.06 | 6.90 | 1.57 | - | 0.23 | 0.24 | 0.16 | 27.12 | 65.39 |
| 3 | 5731.0 | $O_{1\text{-}2}y1$ | 3.46 | 0.01 | 0.34 | 0.04 | 0.01 | 0.29 | 7.2 | 0.08 | 21.21 | 0.90 | 168.4 | 0.01 | 0.12 | 14.51 | 1.24 | 0.003 | 0.30 | 0.63 | 0.08 | 10.18 | 48.67 |
| 4 | 6023.0 | $O_{1\text{-}2}y3$ | 4.15 | 0.00 | 0.32 | 0.05 | 0.02 | 0.45 | 12.0 | 0.10 | 18.58 | 0.76 | 202.1 | 0.01 | 0.14 | 18.30 | 0.66 | 0.002 | 0.46 | 0.89 | 0.16 | 4.59 | 48.70 |
| 5 | 6110.0 | $O_{1\text{-}2}y3$ | 10.79 | 0.02 | 2.11 | 0.13 | 0.08 | 1.58 | 40.3 | 0.32 | 12.91 | 2.63 | 146.0 | 0.03 | 0.38 | 54.89 | 1.78 | 0.088 | 0.91 | 2.59 | 0.17 | 4.69 | 13.53 |
| 6 | 6140.0 | $O_{1\text{-}2}y3$ | 3.70 | 0.00 | - | 0.02 | 0.01 | 0.17 | 6.3 | 0.06 | 17.47 | 1.09 | 126.8 | 0.01 | 0.10 | 10.55 | 0.68 | - | 0.40 | 0.45 | 0.07 | 7.12 | 34.24 |
| 7 | 6161.0 | $O_{1\text{-}2}y3$ | 7.85 | 0.01 | 2.52 | 0.08 | 0.12 | 0.82 | 32.7 | 0.48 | 12.73 | 1.76 | 58.2 | 0.04 | 0.53 | 87.02 | 0.60 | 0.046 | 0.76 | 3.02 | 0.38 | 1.13 | 7.41 |
| 8 | 6184.0 | $O_{1\text{-}2}y3$ | 6.10 | 0.00 | 0.59 | 0.03 | 0.02 | 0.29 | 7.7 | 0.09 | 19.59 | 0.53 | 187.2 | 0.01 | 0.17 | 15.62 | 0.37 | 0.114 | 0.59 | 0.71 | 0.05 | 2.19 | 30.69 |
| 9 | 6192.3 | $O_{1\text{-}2}y3$ | 3.49 | 0.01 | 0.84 | 0.03 | 0.02 | 0.58 | 17.1 | 0.10 | 12.55 | 0.31 | 161.4 | 0.01 | 0.13 | 19.21 | 2.09 | - | 0.40 | 0.76 | - | 16.45 | 46.29 |
| 10 | 6230.0 | $O_{1\text{-}2}y3$ | 2.55 | 0.01 | 0.44 | 0.01 | 0.01 | 0.29 | 31.7 | 0.07 | 13.42 | 0.59 | 106.5 | 0.01 | 0.08 | 12.59 | 1.15 | - | 0.29 | 0.42 | - | 13.68 | 41.80 |
| 11 | 6241.0 | $O_{1\text{-}2}y3$ | 4.23 | 0.00 | 0.10 | 0.01 | 0.02 | 0.12 | 12.7 | 0.06 | 17.78 | 0.69 | 162.1 | 0.01 | 0.10 | 9.99 | 0.45 | - | 0.40 | 0.42 | - | 4.37 | 38.29 |
| 12 | 6316.5 | $O_1y4$ | 3.76 | 0.00 | - | 0.02 | 0.01 | 0.13 | 3.8 | 0.04 | 19.43 | 0.22 | 151.1 | 0.01 | 0.06 | 7.31 | 0.16 | - | 0.29 | 0.31 | - | 2.55 | 40.21 |
| 13 | 6337.0 | $O_{1\text{-}2}y4$ | 5.72 | 0.02 | 0.15 | 0.01 | 0.06 | 0.21 | 11.7 | 0.07 | 12.27 | 0.77 | 145.4 | 0.01 | 0.10 | 13.25 | 1.61 | - | 0.69 | 0.52 | - | 16.05 | 25.43 |
| 14 | 6399.0 | $O_{1\text{-}2}y4$ | 4.57 | 0.00 | 0.34 | 0.03 | 0.03 | 0.27 | 20.9 | 0.12 | 12.71 | 0.52 | 107.3 | 0.01 | 0.20 | 23.68 | 0.56 | - | 0.53 | 0.82 | - | 2.88 | 23.50 |
| 15 | 6429.5 | $O_{1\text{-}2}P$ | 6.49 | 0.03 | 1.13 | 0.02 | 0.05 | 0.47 | 24.2 | 0.27 | 17.05 | 3.88 | 231.8 | 0.02 | 0.23 | 47.67 | 2.05 | 0.034 | 0.49 | 1.59 | 0.09 | 8.87 | 35.72 |
| 16 | 6499.0 | $O_{1\text{-}2}P$ | 16.25 | 0.01 | 3.93 | 0.20 | 0.12 | 2.77 | 22.2 | 0.59 | 12.56 | 1.11 | 105.3 | 0.04 | 0.45 | 107.69 | 0.91 | 0.052 | 1.06 | 5.65 | 0.68 | 2.04 | 6.48 |
| 17 | 6510.0 | $O_{1\text{-}2}P$ | 26.39 | 0.01 | 3.52 | 0.02 | 0.12 | 0.35 | 20.9 | 0.56 | 12.55 | 0.99 | 52.0 | 0.04 | 0.57 | 99.90 | 0.42 | 0.124 | 0.81 | 2.44 | 0.41 | 0.73 | 1.97 |
| 18 | 6520.0 | $O_{1\text{-}2}P$ | 6.02 | 0.01 | 0.70 | 0.02 | 0.02 | 0.47 | 32.7 | 0.13 | 13.14 | 0.70 | 128.8 | 0.01 | 0.14 | 21.12 | 0.24 | 0.005 | 0.28 | 0.74 | 0.01 | 1.70 | 21.40 |
| 19 | 6640.0 | $Є_3xq$ | 3.43 | 0.01 | 0.45 | 0.01 | 0.02 | 0.40 | 106.2 | 0.11 | 12.72 | 1.51 | 50.1 | 0.01 | 0.12 | 19.51 | 1.74 | 0.003 | 0.25 | 0.68 | - | 14.34 | 14.60 |
| 20 | 6643.2 | $Є_3xq$ | 73.48 | 0.07 | 1.06 | 0.01 | 0.02 | 0.16 | 82.9 | 0.05 | 14.04 | 2.17 | 54.8 | 0.01 | 0.10 | 8.98 | 1.41 | 0.013 | 0.28 | 0.24 | - | 13.80 | 0.75 |
| 21 | 6643.5 | $Є_3xq$ | 447.61 | 0.03 | 0.58 | 0.01 | 0.01 | 0.15 | 84.7 | 0.06 | 15.21 | 5.32 | 75.0 | 0.01 | 0.09 | 11.76 | 1.73 | 0.198 | 0.29 | 0.28 | - | 18.59 | 0.17 |
| 22 | 6679.0 | $Є_3xq$ | 4.86 | 0.00 | 1.35 | 0.01 | 0.06 | 0.12 | 381.6 | 0.01 | 20.62 | 0.36 | 51.6 | 0.00 | 0.06 | 2.09 | 0.06 | - | 0.45 | 0.06 | 0.80 | 1.09 | 10.62 |
| 23 | 6724.0 | $Є_3xq$ | 9.90 | 0.00 | 5.36 | 0.01 | 0.00 | 3.92 | 188.0 | 0.01 | 14.95 | 0.28 | 19.7 | 0.00 | 0.05 | 2.26 | 0.28 | - | 3.12 | 0.41 | 0.23 | 5.39 | 1.99 |
| 24 | 6750.0 | $Є_3xq$ | 4.47 | 0.03 | 2.01 | 0.01 | 0.01 | 0.11 | 6.8 | 0.07 | 19.41 | 0.80 | 120.5 | 0.01 | 0.11 | 11.82 | 0.27 | - | 0.57 | 0.42 | 0.00 | 2.51 | 26.93 |
| 25 | 6779.0 | $Є_3xq$ | 20.49 | 0.01 | 0.30 | 0.01 | 0.01 | 0.21 | 147.2 | 0.05 | 13.97 | 2.37 | 55.0 | 0.01 | 0.08 | 8.28 | 0.96 | 0.077 | 0.36 | 0.35 | - | 12.64 | 2.68 |

### Carbon and oxygen isotopes

Limestone or dolomite samples are dried after being powdered (200 mesh) and weighed to approximately 0.5 mg for use. Standard technology of acid digestion is used to obtain carbon in carbonate rocks (Wachter and Hayes 1985). A 0.3~1.0 mg powder sample is reacted with ≥100% phosphoric acid at 72 °C for more than 6 hour to release carbon dioxide (Wachter and Hayes 1985). The oxygen and carbon isotopes of $CO_2$ obtained are measured on an MAT-253 mass spectrometer. A MAT253 stable isotope mass spectrometer is produced by Thermo-Finnigan Company of the United States. The instrument mainly includes five parts: a MAT-253 magnetic separator and ion receiver; three injection-separators, TC/EA, FLASH-EA, Precon; continuous flow interface, confl o III; calculation software of control system, ISODAT, and analytical balance with a relative accuracy of one millionth. Carbon and oxygen isotopes of carbonate ($\delta^{13}$Ccarb and $\delta^{18}$Ocarb) are expressed in "‰" relative to Vienna Pee Dee Belemnite (VPDB). The repeatability of $\delta^{13}$Ccarb and $\delta^{18}$Ocarb is better than ± 0.2 ‰ and ± 0.3 ‰, respectively, based on the laboratory standard and NBS-19 international standard. See Table 1 for these results of carbon and oxygen isotopes.

### Trace element and REE

These samples are cleaned with distilled water and dried naturally. These collected core samples are made into casting sheets. These sheets are observed under a LEICA-DMR Research Grade optical microscope, and then appropriate samples are selected for experiments. These samples are ground to 200 mesh in an agate mortar. Then, approximately 40 mg of powder sample is weighed and placed into the crucible. One milliliter of acetic acid is added at a concentration of 3 mol/l, which reacts with the samples to completion for 12 hour. After the reaction, the solutions are separated centrifugally and then rested. The entire supernatant is removed to another crucible. The residue is dried and weighed, and then the weight of the residue is deducted from the sample weight. The separated supernatant is dried. Then, 0.5 ml nitric acid is added at a concentration of 0.1 mol/l to dissolve the residue and the supernatant is dried again. The same nitric acid is added, and these above operations are repeated until the residual acetic acid is removed. Finally, the supernatant is fixed in 1% nitric acid solution, and "In" is used as an internal standard. Trace elements and REEs are measured in an inductively coupled plasma mass spectrometer (ICP-MS), manufactured by Finnigan Mat company in Germany, at 30 °C with a humidity of 30% relative humidity. These experiments are conducted according to DZ/T0223-2001. The test errors are within 5%, and the results of repeated tests for these same samples are consistent. These results of trace elements and REEs are listed in Table 1 and Table 2, respectively.

## Results

### Lithological characteristics

Tight limestones with a low porosity or permeability are predominantly deposited in the Yijianfang Formation, Tumuxiuk Formation, and the upper of Yingshan Formation. Limestone, dolomitic limestone, dolostone, and calcareous dolostone are developed in the lower of Yingshan Formation, Penglaiba Formation, and the Lower Qiulitag Formation, where reservoirs are superior (Fig. 2 and Fig. 3). Specifically, the Tumuxiuk Formation is characterized by micritic limestone and bioclastic limestone with abundant bioclastic components, such as algae, echinoderms, and bivalves (Fig.4a). The limestones in the Yingshan Formation are primarily composed of grain limestone, micritic limestone, silty crystalline limestone and algal boundstone. Among them, grain limestones are well developed, and the grain sizes are mainly a grade of silty sand under the microscope, accounting for approximately 30%~50%. The peloid without a lamellar structure in Fig. 4b, the oolite with a radial lamellar structure, and the bright aggregate composed of peloid based on Liu et al. (2017) are predominant grain types. Sparite calcarenites were deposited in the upper Ying 3 Member with a size of 1.3 mm. Calcite debris was supported by particles, and the rocks are cemented by calcite (Fig. 4c). The remaining rocks in the Ying 3 Member are mainly fine crystalline dolomite with crystal sizes of matrix dolomite from 0.05 mm to 0.15 mm and a hypidiomorphic-euhedral crystal form. The crystal surface is dirty and flat, with a cloudy center and bright edge structure (Fig. 4d). The proportion of limestones, consisting predominantly of calcisiltite, is larger than that of dolostones in the Ying 4 Member (Fig. 4e). The dolostones in the Ying 4 Member are dominated by fine to medium crystalline dolomite with hypidiomorphic or other crystal structures, curved and dirty crystal surfaces, and intercrystalline contacts between crystals (Fig. 4f). Dolostones are mainly developed in the middle and upper of Penglaiba Formation. The matrix of silty crystalline dolomite is dark gray with a tight structure under the microscope. The size of the crystals is dominated by silty crystals surrounded by argillaceous and organic matter, most of which are not euhedral, with bright surfaces and flat mirrors (Fig. 4g). Limestones are developed in the lower of the Penglaiba Formation. The Lower Qiulitag Formation of the Upper Cambrian is dominated by dolostone. Medium-coarse crystalline dolostones with dolomite fillings and a zonal structure of light and dark alternation can be observed under plane-polarized light. The crystals exhibit blade and saddle shapes (Fig. 4h). Moreover, a small amount of sparite calcarenite exists in the Lower Qiulitag Formation (Fig. 4i).

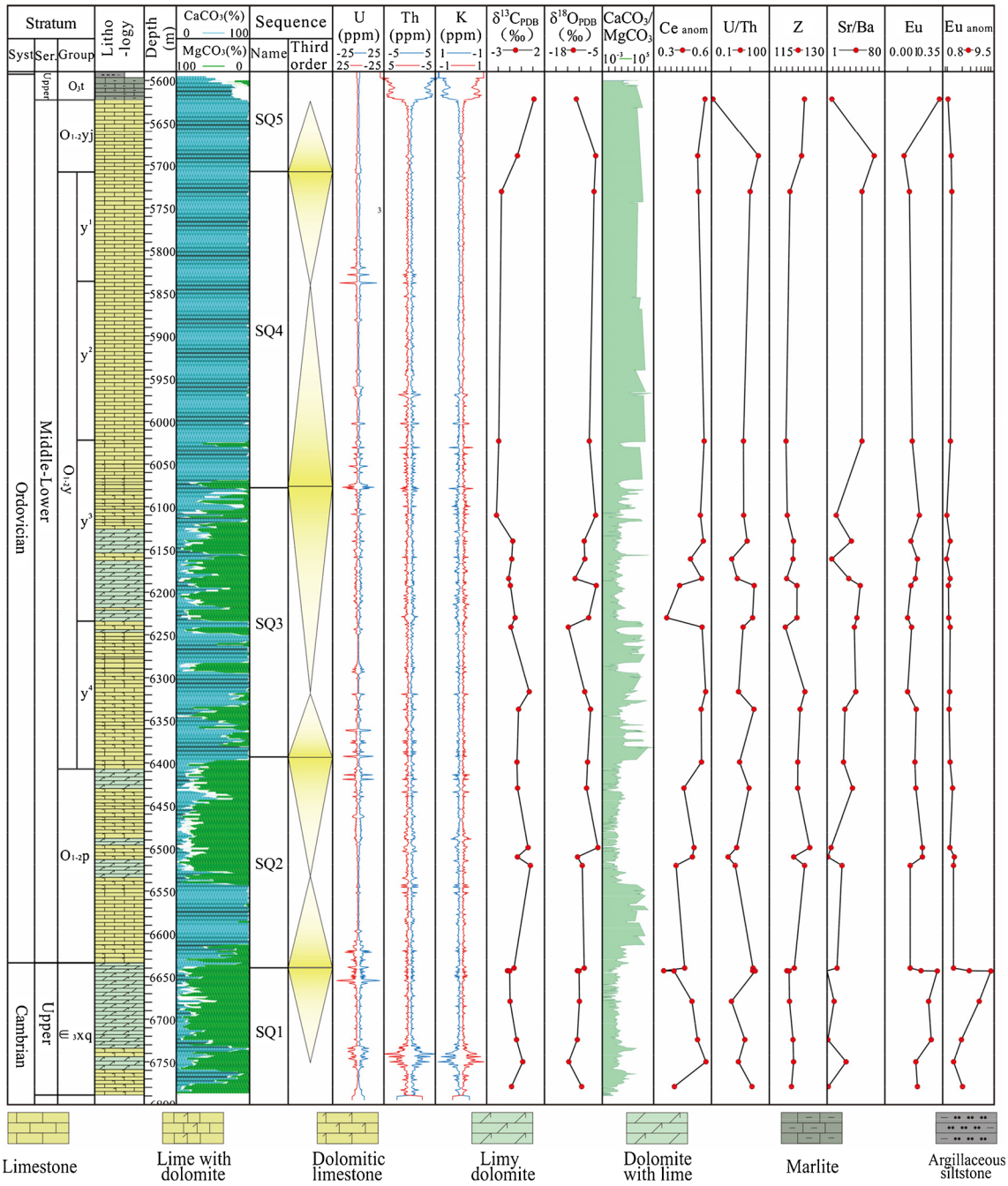


**Fig. 3.** REEs, trace elements and carbon and oxygen isotopes of carbonate in the Paleozoic rocks of GC7 Well with depth. Note: $Ce_{anom}$ = $Ce/Ce^{*}$ = $(3Ce_{PAAS}/(2La_{PAAS}+Pr_{PAAS}))$ (McLennan 1989), PAAS stands for the ratio after PASS standardization; $Eu_{anom}$ $(Eu/Eu^{*}_{PAAS})$ = $Eu_{PAAS}/(Sm_{PAAS} \times Gd_{PAAS})^{1/2}$ (Taylor and Mclennan 1985). In this study, Gd is replaced by Tb in the formula of $Eu_{anom}$

## Carbon and oxygen isotopes

$\delta^{13}$Ccarb values in the Ordovician are mainly between −2.15‰ and 1.09‰, averaging −0.52‰; $\delta^{13}$Ccarb values in the Cambrian vary from −1.20‰ to 0.12‰, averaging −0.71‰ (Table 1). The distribution range of carbon isotopes in the Ordovician of Gucheng area is consistent with that of carbon isotopes of global sea water in the Ordovician (−2‰ ~2‰) (Veizer et al. 1999).

$\delta^{18}$Ocarb values in the Ordovician and Cambrian vary from −12.63‰ to −5.99‰ and from −12.53‰ to −9.06‰, respectively (Table 1). The $\delta^{18}$Ocarb values in the Ordovician are obviously greater than those in the Cambrian. The average $\delta^{18}$Ocarb values of normal marine carbonate rocks are between −10‰ and −2‰ and samples with values below −10‰ are considered unacceptably altered (Kaufman and Knoll 1995). $\delta^{18}$Ocarb values in the Ordovician are mostly greater than −10‰, while $\delta^{18}$Ocarb values in the Cambrian

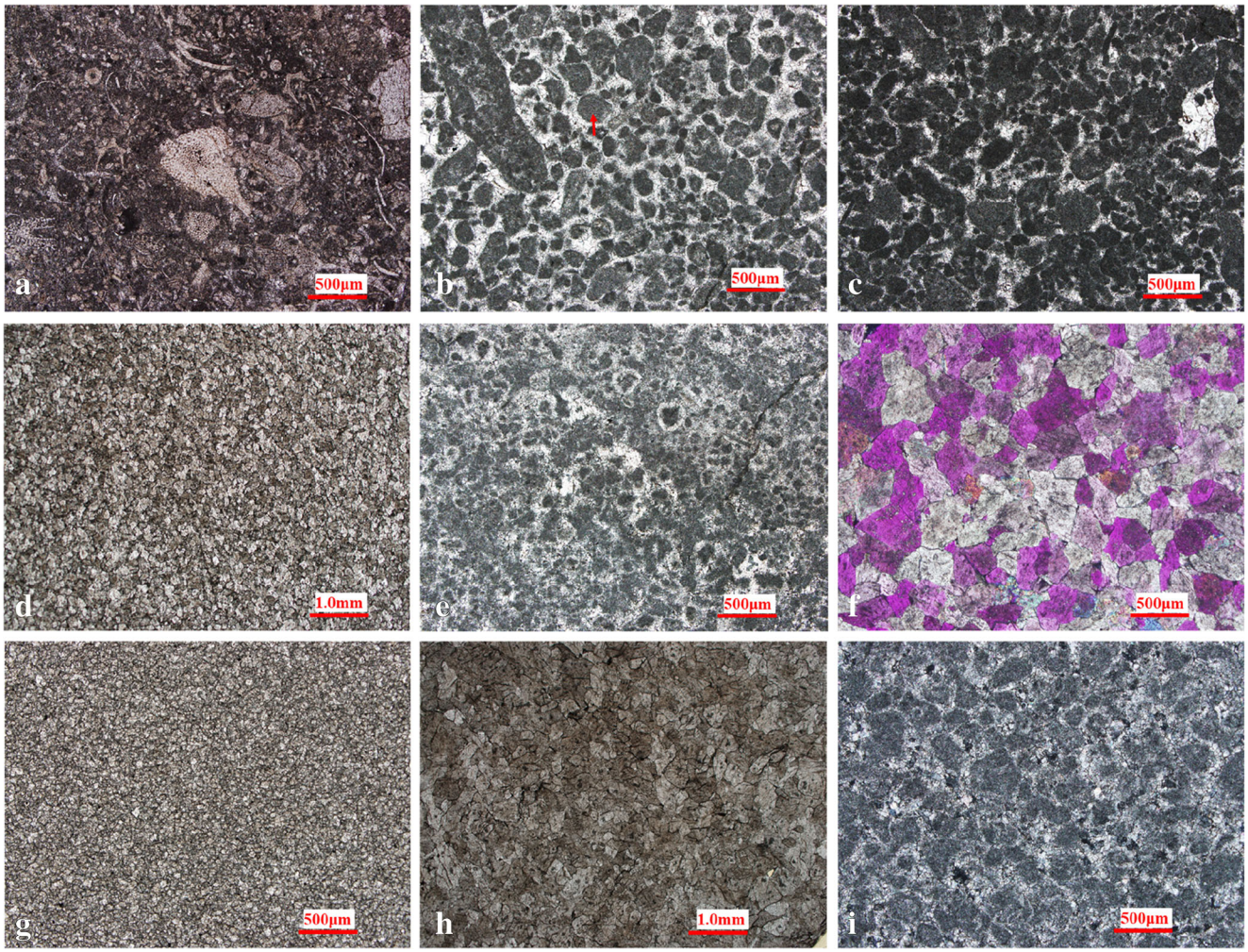


**Fig. 4.** **a** No.1 microcrystalline bioclastic limestone, 5622m, $O_3t$; **b** No.3 sparite calcarenite, 5731, $O_{1\text{-}2}y^1$ (red arrow indicates intraclasts); **c** No.4 sparite calcarenite, 6023m, $O_{1\text{-}2}$ $y^3$; **d** No.7 fine crystalline dolostone, 6161m, $O_{1\text{-}2}$ $y^3$; **e** No.12 sparite calcarenite, 6316.5m, $O_{1\text{-}2}$ $y^4$; **f** No.13 fine-medium crystalline dolostone, 6337m, $O_{1\text{-}2}$ $y^4$; **g** No.16 silty crystalline dolostone, 6499m, $O_{1\text{-}2}p$; **h** No. 22 coarse-medium crystalline dolostone, 6679m, $\in_3xq$; **i** No. 24 sparite calcarenite, 6750m, $\in_3xq$. Pictures a, b, c, d, e, g and h were observed under plane-polarized light; f and i were observed under crossed polarized light

are lower than −10‰, indicating that these samples in the Cambrian are more seriously altered than samples in the Ordovician. The possible causes of alteration are discussed in the fifth section.

## REE + Y

REEs and related parameters of the Lower Paleozoic carbonate rocks are displayed in Table 1. Total REEs (∑REE) range between 0.75 ppm and 32.82 ppm, with an average of 3.85 ppm. Figure 5 shows that the REE + Y distribution pattern based on McLennan (1989) is characterized by a flat distribution and enriched with heavy rare earth elements (HREEs). Overall, more light rare earth elements (LREEs) are lost than HREEs, with $La/Yb_{PASS}$ values from 0.31 to 0.96, causing the curve to tilt left. The LREE/HREEs ratios of carbonate rocks are mostly lower than 1. However, these ratios in the Cambrian are mainly greater than 1, averaging 1.53, with an obvious left-leaning curve. Nd, Sm, and Eu are the main elements in the LREEs, and Y, Tm, and Yb are relatively enriched in the HREEs (Fig. 5). Eu concentrations in the Cambrian, ranging from 0.013 ppm to 0.203 ppm with an average of 0.070 ppm, are obviously significantly higher than the values in the Ordovician with an average of 0.033 ppm, revealing no obvious advantage in the ∑REEs. Nd is significantly higher in the Ordovician, ranging from 0.311 ppm to 12.991 ppm, with an average of 1.795 ppm.

Abnormal Ce ($Ce_{anom}$) is expressed according to the following formula: $Ce_{anom}$ $(Ce/Ce^*_{PAAS}) = (3Ce_{PAAS}/(2La_{PAAS} + Nd_{PAAS}))$. The subscript PAAS in the formula represents the value after the Post-Archean Australian Shale (McLennan 1989). Abnormal Eu ($Eu_{anom}$) is expressed as $Eu_{anom}$ $(Eu/Eu^*_{PAAS}) = Eu_{PAAS}/(Sm_{PAAS} \times Gd_{PAAS})^{1/2}$ (Taylor and Mclennan 1985). In this study, Gd is replaced by Tb in the

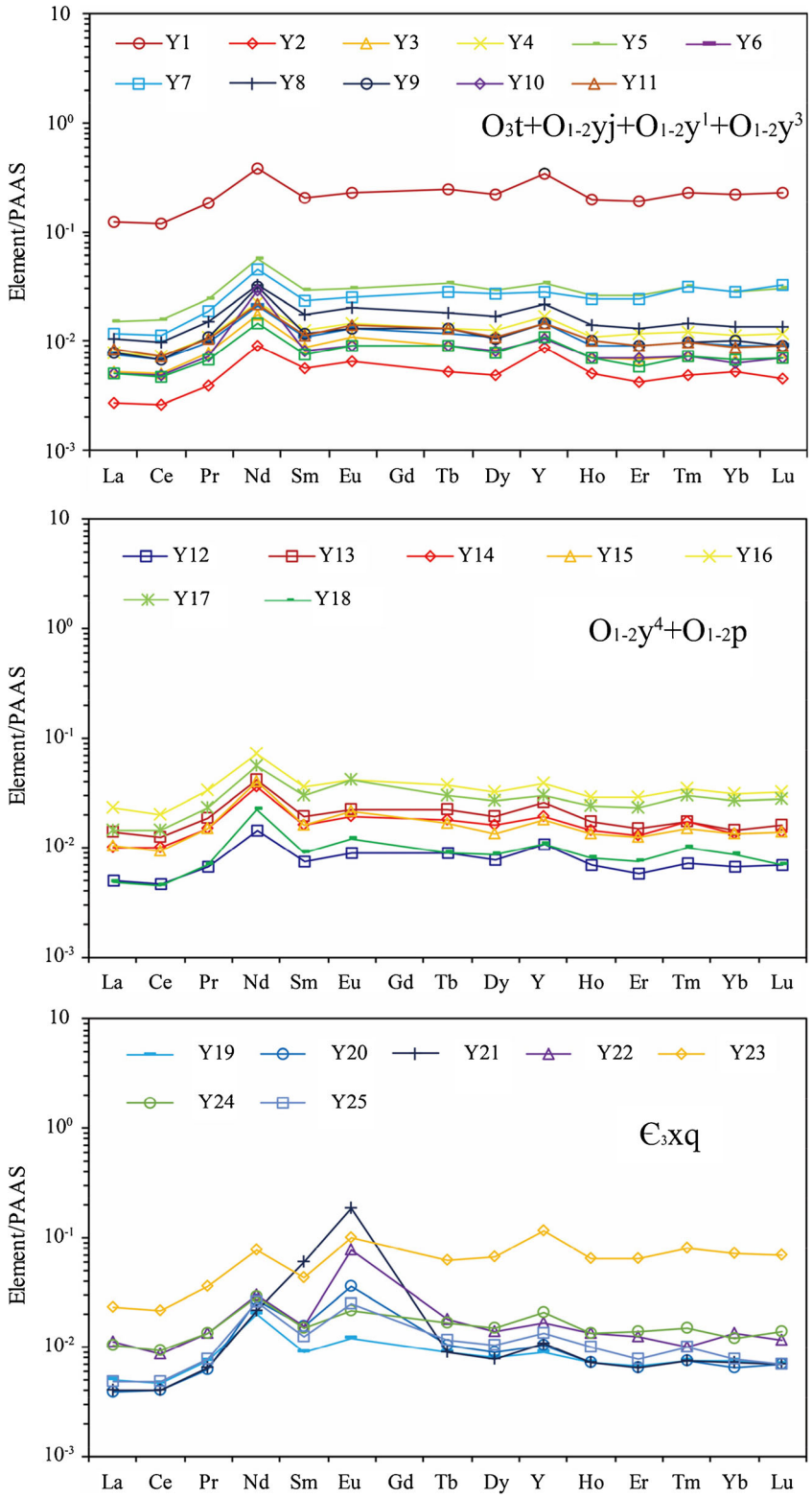


**Fig. 5.** REE+Y distribution pattern of carbonate rocks in the Lower Paleozoic of GC7 Well

formula $Eu_{anom}$. $Ce_{anom}$ values are between 0.35 and 0.57, with an average of 0.50, indicating a negative anomaly. The $Eu_{anom}$ values have a wide distribution range from 0.96 to 8.14, with an average of 1.72. The Cambrian $Eu_{anom}$ is between 1.34 and 8.14, averaging 3.20, which is significantly higher than that in the Ordovician with an average of 1.15.

### Trace elements

The measured values of trace elements and related ratios which are sensitive to the redox environment are listed in Table 2. Among these values, Sr and Mn contents are extremely high, ranging between 20 ppm and 231.8 ppm with an average of 124.9 ppm and between 3.8 and 1010.8 ppm with an average of 94.0 ppm, respectively. The contents of Ba, Cr, Ni, and Ti are also high, ranging from tens to hundreds of ppm. Relatively, the contents of Cd, Cs, Hf, Li, Nb, Pb, Ta, Th, U, W, Y, Rb, and Sc are low, ranging from 0.1 ppm to tens of ppm (Table 2).

The range of U/Th values related to the paleoenvironment is wide, mainly between 0.12 and 27.12, with an average of 7.79. The average value of U/Th in the Cambrian is 9.77, which is slightly greater than that in the Ordovician (7.02). U/Th shows a fluctuating change in the vertical direction. Mn/Ti values in the Ordovician are between 0.20 and 5.52, with an average value of 1.22. These ratios in the Cambrian are mostly greater than 5, with an average value of 43.75, which is significantly greater than that in the Ordovician. These values in the Cambrian and Ordovician show no significant differences. The Sr/Ba values range from 0.17 to 65.39, with an average of 23.80. Sr/Ba values in the Ordovician with an average of 29.85 is greater than those in the Cambrian with an average of 8.25, although some great values exist in the Cambrian.

## Discussion

### Hydrothermal activity

Eu in the REEs is related to hydrothermal activity (Murray et al. 1991; Douville et al. 1999; Guo et al. 2007). A positive anomaly of Eu indicates hydrothermal activity. The REE distribution in hydrothermal solution is dominated by the chemical exchange of plagioclase crystal in the process of ocean crust alteration at a high temperature and pressure (Klinkhammer et al. 1994). In the late stage of volcanism, while Si and Fe are extracted by submarine hydrothermal solution, feldspar is dissolved to release Eu into the hydrothermal solution (Danielson et al. 1992; Klinkhammer et al. 1994). These Cambrian samples show a positive Eu anomaly with $Eu_{anom}$ varying from 1.34 to 8.14, indicating an obvious hydrothermal activity. There is a slight positive Eu anomaly in these Ordovician samples, with an average value of 1.14. Eu values generally decrease gradually from the Cambrian to Ordovician, indicating a decrease in the intensity of hydrothermal activity (Table 1; Fig. 5). Cerium fluoro-carbonate minerals are often related to the intrusion of acidic and alkaline magmatics (Yu et al. 2010). Saddle dolomite cement in the Cambrian of Gucheng area contains cerium fluoro-carbonate minerals (Wang et al. 2016), suggesting an origin of magmatic hydrothermal alteration (precipitation). At the end of the Early Permian, large-scale magmatic intrusion and volcanic eruption occurs in the Tarim Basin, which is caused by the formation of the ancient Tianshan fold belt and the subduction of the Paleotethys ocean (Zhu et al. 2010). Moreover, in the Permian, medium- and small- scale intermediate-acid magmatic rocks are developed in the Gucheng area (Yan et al. 2014). Therefore, high-temperature hydrothermal activity is caused by upwelling magmatic water along a deep and large strike-slip fault closely related to the basement in the Permian. Medium-temperature Cambrian brine is also the hydrothermal fluid present in the Gucheng area based on $^{87}Sr/^{86}Sr$ (Wang et al. 2016).

Oxygen isotopes are used to trace different fluid sources during dolomitization (Chen et al. 2013). The oxygen isotopes of dolomite are mainly controlled by fluid source and temperature (Land 1985; Gasparrini et al. 2006). Higher temperatures can result in less fractionation between fluids and dolomite, leading to lower oxygen isotopes in dolomite; in addition, evaporation and fractionation processes can lead to an increase in oxygen isotopes in seawater, making the oxygen isotope value of evaporated seawater higher than that of normal seawater (Chen et al. 2008; Zheng et al. 2010). Compaction fluids such as modified seawater have an oxygen isotope similar to that of seawater (Chen et al. 2013). Based on the above analysis, Chen et al. (2013) proposed a diagram to judge hydrothermal activity by oxygen isotopes, as shown in Fig. 6. Most likely due to the lack of sufficient data, samples in the Cambrian are all affected by hydrothermal fluids based on Fig. 6. The fluid sources of samples in the Ordovician consist of evaporated seawater, normal seawater, and hydrothermal fluid, suggesting that the samples are controlled by dolomitization during the parasyngenetic period and burial hydrothermal metasomatism dolomitization. By comparison, samples in the Cambrian are more exposed to hydrothermal activity than samples in the Ordovician, which is basically consistent with

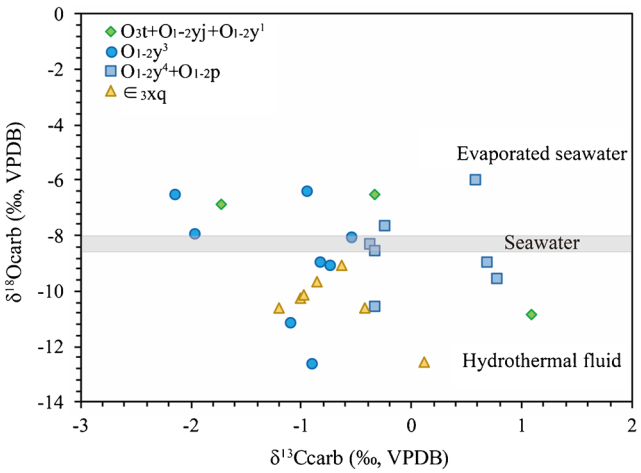


**Fig. 6.** Crossplot of oxygen-carbon isotope of carbonate rocks in the Lower Paleozoic of GC7 Well (the chart based on Chen et al. 2013)

the conclusions of the $Eu_{anom}$ analysis (Fig. 6). Due to the influence of hydrothermal activity, oxygen isotopes in the Cambrian are obviously low, however, the effect on carbon isotopes is little (Chen et al. 2013) (Fig. 6).

## Relative sea level changes

Global long-term (millennium-ten million years) carbon cycle storage is predominantly composed of sedimentary carbonate rock and sedimentary organic matter. They account for 79.952% and 19.994% of the carbon content in the shallow crust and the earth's surface, respectively (Hayes et al. 1999; Hoefs 2004; Sharp 2007) and the sum of dissolved carbon, biological carbon and carbon in the atmosphere only occupies 0.054%. Although carbon content in the mantle and continental siliceous crust is 4.41 times of that in the shallow crust and the earth's surface, the carbon in the former rarely participates in the global carbon cycle, and has little effect on the carbon cycle in the earth's surface. Therefore, it is hardly considered. The average $\delta^{13}C$ values of sedimentary carbonate rock and sedimentary organic matter are 0~1‰ (PDB) and −23 ‰ ~ −25 ‰ (PDB), respectively (Hoefs 2004; Sharp 2007). In other words, carbonate rocks and sedimentary organic matter are enriched in $^{13}C$ and $^{12}C$, respectively. Because the sedimentary organic matter is buried and preserved in the sediments, more $^{12}C$ will be taken away, resulting in the relative enrichment of $^{13}C$ in the hydrosphere, atmosphere and biosphere on the crust surface. This leads to the enrichment of $^{13}C$ or the increased $^{13}C/^{12}C$ ratio ($\delta^{13}C$) in the carbonate rocks and organic matter deposited from the sea (Kump and Arthur 1999; Hoefs 2004). Kaufman and Knoll (1995) considered that the sudden decrease of $\delta^{13}C$ of seawater in the end of Proterozoic from 5‰~10‰ (PDB) to −2‰~ −6‰ (PDB) was related to several glacial periods. Hoffman et al. (1998) believed that this was due to the decrease of the biological productivity and the preservation rate of sedimentary organic matter caused by the ice age (snow ball earth effect).

The preservation rate of sedimentary organic matter is related to the global sea level rise and fall (Tissot 1979). Generally speaking, rising or high global sea level is beneficial to the preservation of sedimentary organic matter, otherwise it is not. Sedimentary organic matter mainly includes marine sedimentary organic matter and coastal swamp coal measures. The high yield and preservation rate are related to greenhouse climate and high global sea level (Tissot 1979). In view of the above isotopic fractionation mechanism, the carbon isotopes of whole rocks or fossil shells of marine carbonate rocks can indicate the relative variation of global sea level (Zhao 2015).

The correlation of carbon and oxygen isotopes can be used to judge whether the carbonate samples are subjected to diagenetic alterations. The more obvious the correlation, the stronger is the diagenetic alteration (Qing and Veizer 1994; Wang and Feng 2002). Figure 6 shows that the carbon and oxygen isotopes have no correlation, which indicates no/weak diagenetic alteration. A loss of Sr and Na and an increase of Fe and Mn occur in the carbonate rocks after the sedimentary period, especially after being affected by the atmospheric water cycle (Veizer 1983; Bruckschen et al. 1995). Hydrothermal fluid from igneous activities which took place in the Tarim Basin in the Permian also leads to the increase of Fe and Mn content and a little loss of Sr content for limestone or dolomite (Jin et al. 2006). Therefore, the Mn/Sr ratio can effectively judge the diagenesis and alteration degree of marine carbonate. Carbonates (both limestone and dolostones) with Mn/Sr < 10 commonly retain near primary $\delta^{13}C$ abundance (Kaufman and Knoll 1995). The Mn/Sr values of carbonate rocks in the GC7 well are less than 10, showing that these carbon isotopes reflect the original marine sedimentary environment. Moreover, the distribution of carbon isotopes is still in the range of normal marine carbonate rocks (−2‰ and 2‰) (Table 1; Fig. 3), which further suggests that these carbon isotopes can be used for geological analysis.

A content of U, Th, and K in the natural gamma-ray spectral logging is highly sensitive to the change of sedimentary environment. Due to the weathering, a clay layer is formed on an exposed surface. Th with high stability during weathering is insoluble in water and is relatively enriched near an exposed surface; K is easily soluble in water to be transported away (Zheng et al. 2004; Gao et al. 2016). U is usually enriched in clay to indicate an elevation of base level; carbonate rocks tend to fracture and be eroded, which leads to an increased U content near a sequence boundary caused by the mud filling in the dissolved pores/cavities or fractures (Wang et al. 2008). According to the characteristics of the seismic and logging in this area and the research of Lin et al. (2017), 5 third-order sequence (SQ) are identified in the Upper Cambrian and Ordovician. The interface of SQ1 and SQ2 is corresponding to the boundary of Cambrian and Ordovician. The SQ2 and SQ3 are roughly separated by the boundary between the Penglaiba and Yingshan Formations, which is a parallel unconformity as a whole. The SQ3 and SQ4 boundary roughly is the interface between the upper and lower of Yingshan Formation. This interface is eroded due to the middle Caledonian movement (Cai and Li 2008), but it is well preserved in the Gucheng area as a parallel unconformity. The SQ4 and SQ5 roughly corresponds to the boundary between the Yingshan and Yijianfang Formations (Liu et al. 2017). The variation trend of carbon isotopes in this study is basically consistent with that of carbon isotopes proposed by Veizer et al. (1999), i.e., lighter in the Late Cambrian, stable in the Early Ordovician, and rapidly increasing in the Middle-Late Ordovician, revealing the rationality of these carbon isotopes. $\delta^{13}Ccarb$ in the Late Cambrian changes from a positive to a negative deviation as the depth increases, indicating that the relative sea level drops. From limestone in the Penglaiba

Formation to dolomite in the Penglaiba Formation to limestone of the Ying 4 Member to dolomite of the Ying 3 Member, the relative sea level shows a rise-drop-rise-drop trend. In the Upper Ordovician, the water body generally rises due to lack of sufficient data in the upper of Yingshan Formation. Dolomite and limestone are developed in the regression and transgression periods, respectively (Fig. 3). The relative sea level fluctuations based on the carbon isotopes is basically consistent with identified sequences in the Gucheng area, indicating that the relative rise-fall of sea level controls the sequence evolution (Fig. 3). The SQ1 with a half cycle in the upper of Qiulitage Formation, SQ2 in the Penglaiba Formation and SQ3 in the lower of Yingshan Formation, which are dominated by sea-level decline cycle, are more likely to develop restricted platform (Fig. 7). With the decrease of sea level, the thickness and content of dolomite increase, and the distribution expands to the platform margin. The sedimentary environment of SQ4 in the upper of Yingshan Formation and SQ5 in the Yijianfang Formation, which are dominated by sea-level rise, has changed to open platform. Moreover, dolomite thickness and content decrease, and the distribution of open platform increases (Fig. 7).

The relative sea level change is a combined action of tectonic fluctuation in the specific area (or basin) and global sea level change (Zhu 2000). Haq and Schutter (2008) reconstructed a history of sea-level fluctuations for the entire Paleozoic by using stratigraphic sections from pericratonic and cratonic basins, which shows a gradual rise during the Cambrian, reaching a zenith in the Late Ordovician. The Tarim Basin has experienced a passive continental margin (expansion activities) in the Cambrian-Early Ordovician, and squeezing activities during the Middle-Late Ordovician (Yu et al. 2011). The relative change of sea level based on carbon isotope and third-order sequence depends on global sea level change obtained by Haq and Schutter (2008) combined with tectonic uplift of the Tarim Basin proposed by Yu et al. (2011), which leads to a gradual rise during the Cambrian-Early Ordovician and a gradual drop during the Middle-Late Ordovician in the Gucheng area.

## Paleosalinity

Variations of $\delta^{18}O$ and $\delta^{13}C$ in the carbonate and cement of clastic rock indicate a sedimentary diagenetic environment (Kuleshov and Bych 2002; Aranovich et al. 2010). $\delta^{13}C$ values are between −1‰ and −2‰ in the ocean with high salinity and between −5 ‰ and −11 ‰ in fresh water. The $\delta^{18}O$ values in seawater are approximately 0 and not greater than 1‰. The $\delta^{18}O$ values of fresh water caused by atmospheric precipitation are lower than 0, with a lowest value of −50‰ (Gao et al. 2012). Both $\delta^{18}$Ocarb and $\delta^{13}$Ccarb values are related to the salinity of water body, and the higher the salinity, the higher are these isotope values (Epstein and Mayeda 1953; Clayton and Degens 1959; Zhang 1985). Previous research has comprehensively analyzed carbon and oxygen isotopes to indicate paleosalinity and proposed an equation to calculate paleoseawater salinity for distinguishing marine and freshwater carbonate rocks in the Jurassic and newer strata: $Z = 2.048\ (\delta^{13}C_{carb}+50) + 0.498\ (\delta^{18}O_{carb}+50)$ (Keith and Weber 1964). In the formula, the Z value is affected by salinity. Z value greater than 120 suggests that carbonate rock is of seawater origin. Z value lower than 120 represents a freshwater origin of carbonate rock. When Z value equals 120, it is undefined carbonate rock. Moreover, Z value is widely used in the paleosalinity analysis of Paleozoic and Cenozoic carbonate rocks in China, as described by Xu et al. (2009).

Fresh water is characterized by strong acidification and a low mineralization degree, which lead to a small content of $SO_2^{-4}$, and Sr and Ba are retained in the water in the form of ions. In the salinization process of lake water, Ba first precipitates in the form of $BaSO_4$ with increasing salinity. Sr precipitates only when the salinity of water reaches a certain degree (Deng and Qian 1993; Zheng et al. 2015). Therefore, the Sr/Ba value is an indicator for distinguishing the sedimentary environment and water salinity (Deng and Qian 1993; Liu et al. 2007; Zheng et al. 2015). A higher Sr/Ba ratio suggests a higher paleosalinity and dry-cold climate. Sr/Ba greater than 1 indicates marine salt water and a ratio between 0.6 and 1 indicates transitional facies; a ratio lower than 0.6 suggests continental freshwater deposition (Geology of Nanjing University 1979; Deng and Qian 1993; Wu 2001; Zheng et al. 2015).

Z values of these samples in the Ordovician are predominantly more than 120, indicating that carbonate rocks in the Lower Paleozoic are marine origin (Table 1). Therefore, Z values are still indicative significance in the study area. Because Z values are proposed to distinguish fresh water and marine limestone in the Jurassic and newer strata by Keith and Weber (1964), it is essential to determine whether the Z value can be used to explain the variation of paleosalinity for samples in the Ordovician quantitatively. Z values decrease overall from the Upper Cambrian to the Ordovician, indicating a decrease in salinity. Moreover, Z values of limestones with high values of $CaCO_3/MgCO_3$ in the Penglaiba Formation, Ying 4 Member, and Middle-Upper Ordovician are significantly lower than those of dolomites with low $CaCO_3/MgCO_3$ values, suggesting that the limestones are deposited in a low salinity environment compared with the dolomites (Fig. 3; Table 1).

Sr/Ba ratio in the $\in_3$xq and Ordovician are mostly greater than 1, which also indicates marine salt water. Paleosalinity variation with depth based on Sr/Ba values contrasts with the conclusions obtained for paleosalinity in view of Z values and is inconsistent with the paleoenvironment and paleodepth research. The possible reasons are as follows. Sr is preferentially partitioned into Na- and Ca-rich minerals, such as carbonates,

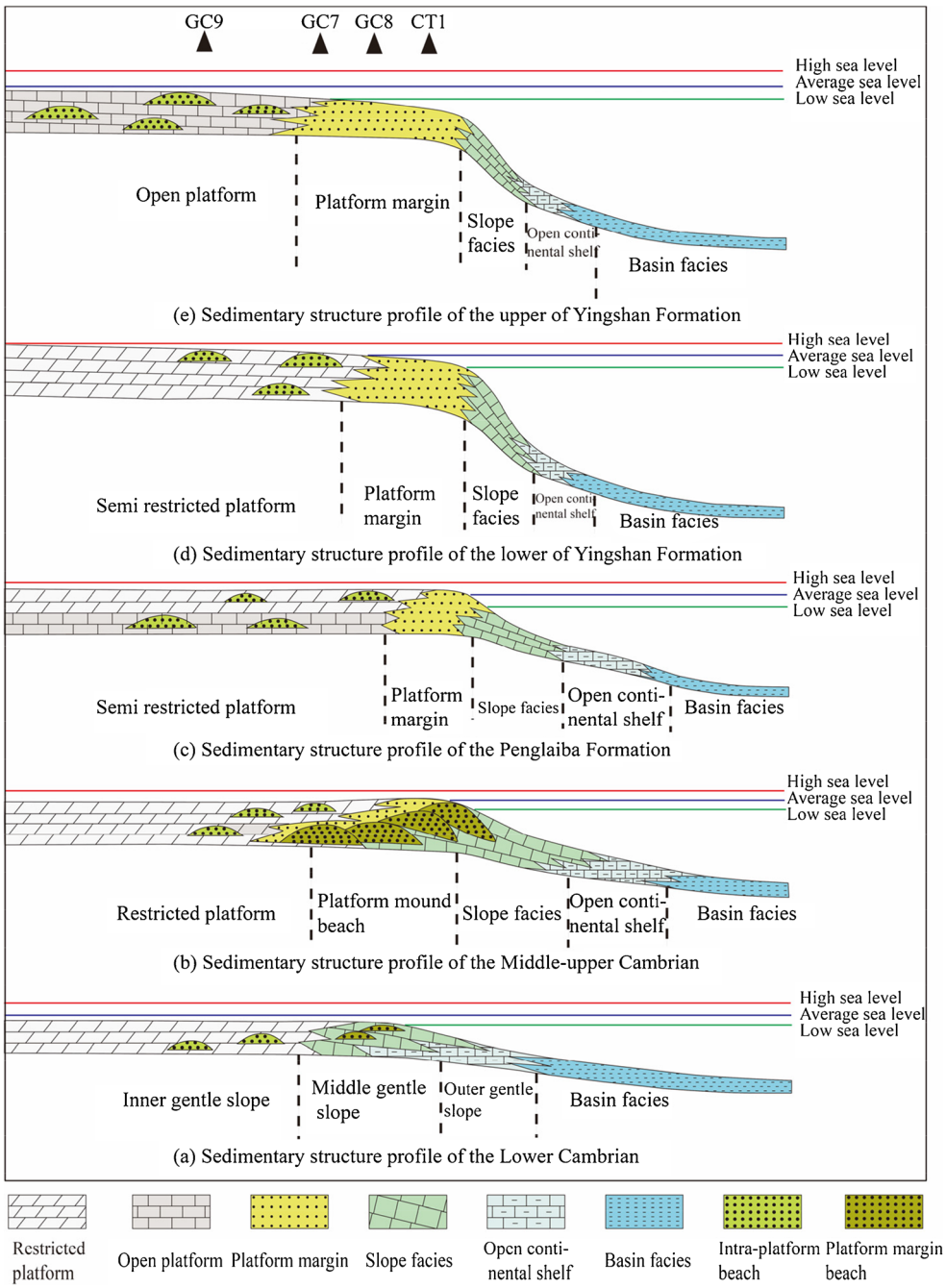


**Fig. 7.** Sedimentary evolution model of the Cambrian and Ordovician carbonate rocks in the Gucheng area

plagioclase, and amphibole (Chen et al. 1999). Therefore, Sr/Ba is controlled by the $CaCO_3$ content (Liu and Cao 1987; Sun et al. 2000), which suggests that Sr/Ba is not applicable to research the paleosalinity of marine carbonate in the study area.

## Paleoredox environment

U, V, Co, Ni, Zn, Cd, and Cr are redox sensitive elements with various valence states. The valence states of these elements are affected by the oxidation-reduction environment when they are deposited (Morford and Emerson 1999; Tribovillard et al. 2006). Ti and Th are mainly derived from terrigenous weathering and have difficulty migrating in secondary processes (Calvert and Pedersen 1993; Tribovillard et al. 1994; Hild and Brumsack 1998; Böning et al. 2004), which are applied to indicate land source input flux. Figure 8 shows that the correlation indices ($R^2$) between Ti and U and between Th and U are 0.0427 and 0.0116, respectively, indicating poor correlations between these elements. Therefore, carbonate rocks are not affected by terrigenous sources. The valence states of U are mainly +6 and +4. In water with oxygen, U

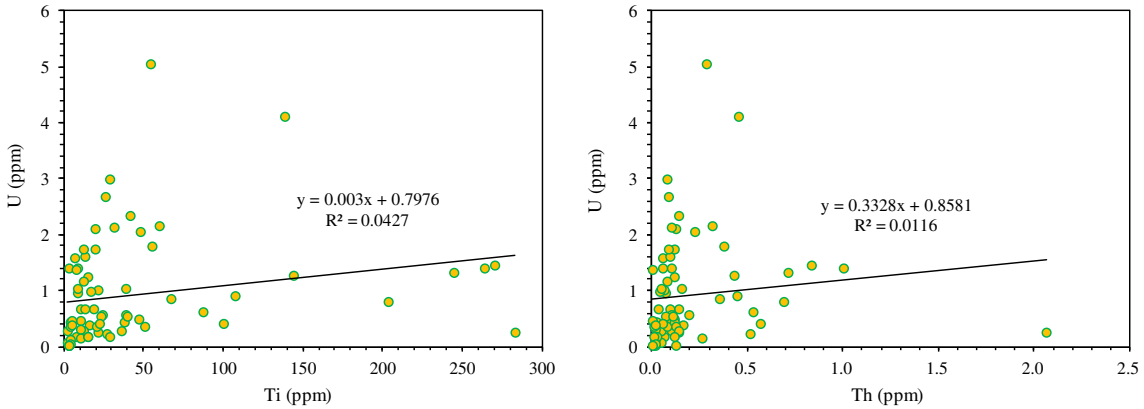


**Fig. 8.** Relationship between U value and Ti and Th of carbonate rocks in the Lower Paleozoic

is usually +6 and forms a stable complex, i.e., $[UO^2(CO_3)_3]^{4-}$, with carbonate ions in the form of uranyl (Langmuir 1978; Anderson et al. 1989; Kimura and Watanabe 2001). In a reducing environment, U with +6 is reduced to insoluble U with +4 (Jones and Manning 1994; Wignall and Twitchett 1996; Mcmanus et al. 2005). U/Th can indicate a redox environment (Adams and Weaver 1958; Rogers and Adams 1969; Jones and Manning 1994). A higher U/Th ratio suggests a stronger reducibility of the paleoenvironment. Generally, anoxic and hypoxic environments are separated by a U/Th of 1.25; oxidized and hypoxic environments are distinguished by a U/Th of 0.75 (Jones and Manning 1994).

Ce records the redox state of the water body and is also preserved during subsequent burial and diagenesis (Wright et al. 1987; German and Elderfield 1989; De Baar et al. 1988). Therefore, Ce can be applied to distinguish the redox condition of paleoenvironment. $Ce^{3+}$ in seawater is easily oxidized to $Ce^{4+}$ and then adsorbed by oxide colloids such as iron and manganese under oxidation conditions. $Ce^{4+}$ is reduced to $Ce^{3+}$ and then released, resulting in the enrichment of Ce in seawater and the loss of Ce in sediment with the dissolution of oxides such as iron and manganese under a reducing conditions (Wright et al. 1987; German and Elderfield 1989; De Baar et al. 1988). The positive and negative anomalies of Ce suggests a reducing and oxidizing environment, respectively (Wright et al. 1987). However, later diagenes tend to indicate a positive correlation of $Ce_{anom}$ with ∑REE and a negative correlation with $Dy_{PASS}/Sm_{PASS}$ (Shields and Stille 2001). Figure 9 shows a poor correlation between $Ce_{anom}$ and the two parameters, indicating a minor impact of diagenesis on REEs. Therefore, Ce and other elements can judge the paleoenvironment of carbonate rocks. In this study, U/Th, $Ce_{anom}$, and $CaCO_3/MgCaCO_3$ in the logging are applied to comprehensively analyze the oxidation and reduction environment.

The change in the U/Th and $Ce_{anom}$ values of the Lower Paleozoic carbonate rocks with depth show that the U/Th values are mostly greater than 1.25. It seems that the carbonate rocks are deposited in anoxic environments (Fig. 3). However, $Ce_{anom}$ values range from 0.3 to 0.6 and are all lower than 1, showing negative anomalies, i.e., an oxidation environment, which is contrary to the conclusion inferred by U/Th values. Geologic exploration shows that carbonate rocks in the Ordovician are reservoirs and caprocks of hydrocarbon, and source rocks are located in the Middle-Lower Cambrian (Zhou et al. 2019). Moreover, the average total organic carbon

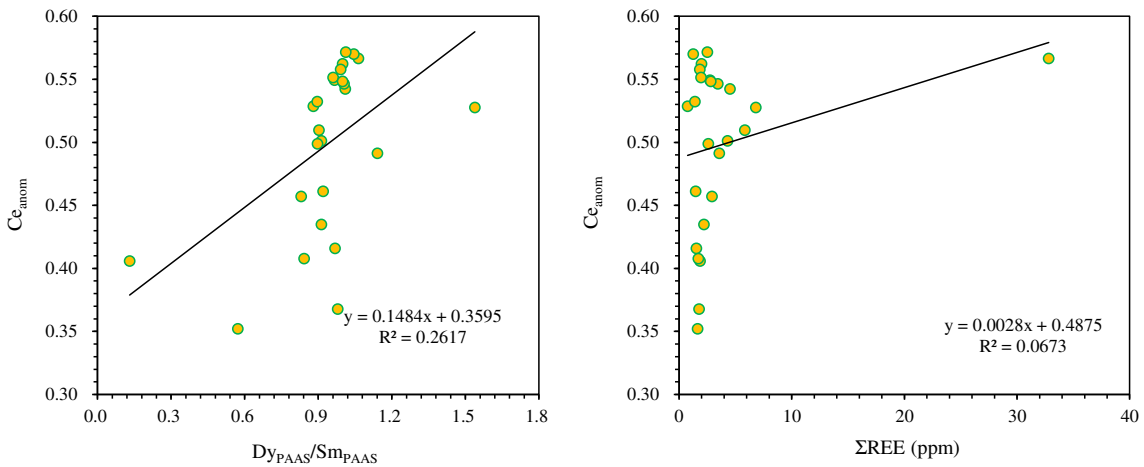


**Fig. 9.** Relationship between $Ce_{anom}$ and $Dy_{PAAS}/Sm_{PAAS}$ and ∑REE of carbonate rocks in the Lower Paleozoic

(TOC) content of the Ordovician carbonate rocks (5300-6500 m) at the GC7 well is approximately 0.2%, indicating non-source rock (Cai 2014). Comprehensive analysis shows that carbonate rocks are deposited in an oxidizing environment, consistent with the analysis result of $Ce_{anom}$ rather than that of U/Th. The reason that the U/Th value cannot be used to indicate the sedimentary environment in this area may be that the solution pores/caves or fractures under the sequence boundary are filled with mud rich in U and Th, which can't be applied to research the sedimentary environment (Liu et al. 2017). The $Ce_{anom}$ values in these dolomites are generally lower than those in limestones and are positively correlated with the $CaCO_3$ content (Fig. 3), which indicates that the dolomites are deposited in a stronger oxidation environment than the limestones are. Therefore, compared with the limestones, the dolomites form in a paleoenvironment with a high salinity, a strong oxidation and a low sea level.

## Conclusions

The sedimentary environment of the Lower Paleozoic carbonate rocks in the Gucheng area is discussed based on the analysis of carbon and oxygen isotopes, trace elements and REEs. Conclusions are drawn as follows.

(1) Both $Eu_{anom}$ and the chart of carbon and oxygen isotopes show that the carbonate rocks in the Upper Cambrian and Ordovician are affected by hydrothermal activity. Compared with Ordovician rocks, the Upper Cambrian rocks exhibit obvious hydrothermal activity, which leads to low oxygen isotopes. High-temperature hydrothermal fluid is originated from magmatic water in the Permian.

(2) The carbon isotopes are hardly affected by diagenesis and hydrothermal process. The carbonate rocks in the Upper Cambrian and Ordovician are divided into five third-order sequences based on carbon isotopes and natural gamma-ray spectral logging combined with previous researches. The SQ1, SQ2, and SQ3 are dominated by sea-level decline cycles; SQ4 and SQ5 take sea-level rise cycles as primary.

(3) Z values indicate carbonate deposition with the most values greater than 120 and are used for quantitatively analyzing paleosalinity. The paleosalinity decreases from the Upper Cambrian to the Upper Ordovician according to Z values. Compared with dolomite, limestones are deposited in a low salinity environment based on Z values lower than those of dolomites. The Sr/Ba value is not appropriate for qualitative paleosalinity research of carbonate rocks.

(4) $Ce_{anom}$ values shows the Lower Paleozoic carbonate rocks are deposited in an oxidation environment. Moreover, the dolomites are formed in a paleoenvironment with a higher salinity, a stronger oxidation and a lower falling sea level than that of the limestones.

**Funding** This study was financed by the postdoctoral research fund of shengli oilfield, Sinopec.

**Data Availability** All the data analyzed during this study are included in this manuscript.

## Declarations

**Conflict of interest** The author(s) declare that they have no competing interests.

## References

Adams JAS, Weaver CE (1958) Thorium-to-uranium ratios as indicators of sedimentary processes; example of concept of geochemical facies. Am Assoc Pet Geol Bull 42(2):387–430. https://doi.org/10.1306/0BDA5A89-16BD-11D7-8645000102C1865D

Akinlua A, Sigedle A, Buthelezi T, Fadipe OA (2015) Trace element geochemistry of crude oils and condensates from South African Basins. Mar Pet Geol 59:286–293. https://doi.org/10.1016/j.marpetgeo.2014.07.023

Akinlua A, Olise FS, Akomolafe AO, McCrindle RI (2016) Rare earth element geochemistry of petroleum source rocks from northwestern Niger Delta. Mar Pet Geol 77:409–417. https://doi.org/10.1016/j.marpetgeo.2016.06.023

Anderson RF, Fleisher MQ, Lehuray AP (1989) Concentration, oxidation state, and particulate flux of uranium in the Black Sea. Geochim Cosmochim Acta 53(9):2215–2224. https://doi.org/10.1016/0016-7037(89)90345-1

Aranovich LY, Dubinina EO, Avdeenko AS, Lebedeva YM, Bushmin SA, Dolivo-Dobrovol'skii DD (2010) Oxygen isotopic composition of coexisting minerals of sillimanite-hypersthene rocks from the Por'ya bay area: Evidence of fluid involvement in granulite-facies metamorphism. Geochem Int 48(8):739–751. https://doi.org/10.1134/S001670291008001X

Böning P, Brumsack HJ, Böttcher ME, Schnetger B, Kriete C, Kallmeyer J, Borchers SL (2004) Geochemistry of Peruvian near-surface sediments. Geochim Cosmochim Acta 68(21):4429–4451. https://doi.org/10.1016/j.gca.2004.04.027

Bruckschen P, Bruhn F, Meijer J, Stephan A, Veizer J (1995) Diagenetic alteration of calcitic fossil shells: Proton microprobe (PIXE) as a trace element tool. Nucl Instrum Methods Phys Res, Sect B 104(1-4):427–431. https://doi.org/10.1016/0168-583X(95)00424-6

Cai YW (2014) Source rock analysis and evaluation in the Eastern part of Tarim Basin. A dissertation of China university of Geosciences for Master Degree 1-87 (in Chinese with English abstract)

Cai XY, Li Y (2008) Ordovician lithfacies and stratigraphic lacunae in southern part of central Tarim, Xinjiang. J Stratigr 32(4):353–362

Cai XY, Li HL, Ma YC, You DH (2006) Characteristic of sedimentary facies of Guchengxu uplift Ordovician at Tarim Basin. Journal of Central South University (Science and Technology) 37(1):155–161 (in Chinese with English abstract). https://doi.org/10.1016/S1874-8651(10)60080-4

Calvert SE, Pedersen TF (1993) Geochemistry of recent oxic and anoxic marine sediments: implications for the geological record. Mar Geol 113(1-2):67–88. https://doi.org/10.1016/0025-3227(93)90150-T

Cao J, Wu M, Chen Y, Hu K, Bian LZ, Wang LG, Zhang Y (2012) Trace and rare earth element geochemistry of Jurassic mudstones in the northern Qaidam Basin, northwest China. Chemie der Erde-Geochemistry 72(3):245–252. https://doi.org/10.1016/j.chemer.2011.12.002

Cao YH, Wang S, Zhang YJ, Yang M, Yan L, Zhao YM, Zhang JL, Wang XD, Zhou XX, Wang HJ (2019) Petroleum geological conditions and exploration potential of Lower Paleozoic carbonate rocks in Gucheng Area, Tarim Basin, China. Pet Explor Dev 46(6):1165–1181. https://doi.org/10.1016/S1876-3804(19)60271-5

Chen J, An ZS, Head J (1999) Variation of Rb/Sr ratios in the loess-paleosol sequences of Central China during the last 130,000 years and their implications for monsoon paleoclimatology. Quat Res 51(3):215–219. https://doi.org/10.1006/qres.1999.2038

Chen YQ, Zhou XY, Zhao KD, Yang WJ, Dong CY (2008) Geochemical research on straticulate dolostone and spatulate dolostone in Lower Ordovician strata of Tazhong1 Well, Tarium Basin. Acta Geol Sin 82(6):826–834

Chen YQ, Zhou XY, Jiang SY, Zhao KD (2013) Types and Origin of Dolostones in Tarim Basin, Northwest China: Petrographic and Geochemical Evidence. Acta Geologica Sinica - English Edition 87(2):467–485. https://doi.org/10.1111/1755-6724.12062

Clayton RN, Degens ET (1959) Use of carbon isotope analyses of carbonates for differentiating fresh-water and marine sediments. Am Assoc Pet Geol Bull 43(4):889–897. https://doi.org/10.1306/0BDA5CF6-16BD-11D7-8645000102C1865D

Danielson A, Moller P, Dulski P (1992) The europium anomalies in banded iron formation and the thermal history of the oceanic crust. Chem Geol 97(1-2):89–100. https://doi.org/10.1016/0009-2541(92)90137-T

De Baar HJW, German CR, Elderfield H, van Gaans P (1988) Rare earth element distributions in anoxic waters of the Cariaco Trench. Geochim Cosmochim Acta 52(5):1203–1219. https://doi.org/10.1016/0016-7037(88)90275-X

Deng HW, Qian K (1993) Sedimentary geochemistry and environmental analysis. Gansu science and Technology Press, Lanzhou, pp 1–104

Douville E, Bienvenu P, Charlou JL, Donval JP, Fouquet Y, Appriou P, Gamo T (1999) Yttrium and rare earth elements in fluids from various deep-sea hydrothermal systems. Geochim Cosmochim Acta 63(5):627–643. https://doi.org/10.1016/S0016-7037(99)00024-1

Epstein S, Mayeda TK (1953) Variation of O-18 Content of Waters from Natural Sources. Geochim Cosmochim Acta 4:213–224. https://doi.org/10.1016/0016-7037(53)90051-9

Frimmel HE (2009) Trace element distribution in Neoproterozoic carbonates as palaeoenvironmental indicator. Chem Geol 258(3-4):338–353. https://doi.org/10.1016/j.chemgeo.2008.10.033

Gao SL, Wang LM, Wu X, Li ZM, Gao PP (2012) Geochemical Characteristics and Dicussion on Related Problems of Sha 1 Submember Carbonate Reservoirs in the Qijiawu Area in Huanghua Depression. Acta Geol Sin 86(10):1688–1695 (in Chinese with English abstract)

Gao D, Lin CS, Hu MY, Gao LL (2016) Using spectral gamma ray log to recognize high-frequency sequence in carbonate strat: a case study from the Lianglitege formation from well T1 in Tazhong area, Tarim basin. Acta Sedimentol Sin 34(4):707–715. https://doi.org/10.14027/j.cnki.cjxb.2016.04.011

Gasparrini M, Bechstädt T, Boni M (2006) Massive hydrothermal dolomites in the southwestern Cantabrian Zone (Spain) and their relation to the Late Variscan evolution. Mar Pet Geol 23(5):543–568. https://doi.org/10.1016/j.marpetgeo.2006.05.003

Geology of Nanjing University (1979) Geochemistry. Sicence Press, Beijing, pp 339–364 (in Chinese)

German CR, Elderfield H (1989) Rare earth elements in Saanich Inlet, British Columbia, a seasonally anoxic basin. Geochim Cosmochim Acta 53(10):2561–2571. https://doi.org/10.1016/0016-7037(89)90128-2

Guo QJ, Shields GA, Liu CQ, Strauss H, Zhu MY, Pi DH, Goldberg T, Yang XL (2007) Trace element chemostratigraphy of two Ediacaran-Cambrian successions in South China: implications for organosedimentary metal enrichment and silicification in the early Cambrian. Palaeogeogr Palaeoclimatol Palaeoecol 254(1-2):194–216. https://doi.org/10.1016/j.palaeo.2007.03.016

Haq BU, Schutter SR (2008) A chronology of Paleozoic sea-level changes. Science 322:64–68. https://doi.org/10.1126/science.1161648

Hayes JM, Strauss H, Kaufman AJ (1999) The abundance of $^{13}C$ in marine organic matter and isotopic fractionation in the global biogeochemical cycle of carbon during the past 800Ma. Chem Geol 161(1/3):103–125. https://doi.org/10.1016/S0009-2541(99)00083-2

Hild E, Brumsack HJ (1998) Major and minor element geochemistry of Lower Aptian sediments from the NW German Basin (core Hohenegglesen KB 40). Cretac Res 19(5):615–633. https://doi.org/10.1109/ECWT.2006.280501

Hoefs J (2004) Stable isotope geochemistry [M]. Springer Verlag, Berlin, pp 1–240

Hoffman PE, Kaufman AJ, Halverson GP, Schrag DP (1998) A Neoproterozoic snowball earth. Science 281(5381):1342–1346. https://doi.org/10.1126/science.281.5381.1342

Jia CZ (1999) Structural characteristics and oil/gas accumulative regularity in Tarim Basin. Xinjiang Petroleum Geology 20(3):177–183 (in Chinese with English abstract)

Jin ZJ, Zhu DY, Hu WX, Zhang XF, Wang Y, Yan XB (2006) Geological and geochemical signatures of hydrothermal activity and their influence on carbonate reservoir beds in the Tarim Basin. Acta Geol Sin 80(2):245–253

Jones BJ, Manning AC (1994) Comparison of geochemical indices used for the interpretation of palaeoredox conditions in ancient mudstones. Chem Geol 111(1-4):111–129. https://doi.org/10.1016/0009-2541(94)90085-X

Kaufman AJ, Knoll AH (1995) Neoproterozoic variations in the C-isotopic composition of seawater: stratigraphic and biogeochemical implications. Precambrian Res 73(1-4):27–49. https://doi.org/10.1016/0301-9268(94)00070-8

Keith ML, Weber JN (1964) Carbon and oxygen isotopic composition of selected limestones and fossils. Geochim Cosmochim Acta 28(10-11):1787–1816. https://doi.org/10.1016/0016-7037(64)90022-5

Kimura H, Watanabe Y (2001) Ocean anoxia at the Precambrian-Cambrian boundary. Geology 29(11):995–998. https://doi.org/10.1130/0091-7613(2001)0292.0.CO;2

Klinkhammer GP, Elderfield H, Edmond JM, Mitra A (1994) Geochemical implications of rare earth element patterns in hydrothermal fluids from mid-ocean ridges. Geochim Cosmochim Acta 58(23):5105–5113. https://doi.org/10.1016/0016-7037(94)90297-6

Kuleshov VN, Bych AF (2002) Isotopic composition ($\delta^{13}C$, $\delta^{18}O$) and origin of manganese carbonate ores of the usa deposit (Kuznetskii Alatau). Lithol Miner Resour 37(4):330–343. https://doi.org/10.1023/A:1019995322515

Kump LR, Arthur MA (1999) Interpreting carbon-isotope excursions: carbonates and organic matter. Chem Geol 161(1-3):181–198. https://doi.org/10.1016/S0009-2541(99)00086-8

Land LS (1985) The origin of massive dolomite. J Geol Educ 33(2):112–125. https://doi.org/10.5408/0022-1368-33.2.112

Langmuir D (1978) Uranium solution-mineral equilibria at low temperatures with applications to sedimentary ore deposits. Geochim Cosmochim Acta 42(6):547–569. https://doi.org/10.1016/0016-7037(78)90001-7

Li A, Ju LB, Zhang LY (2018) Relationship between hydrocarbon accumulation and Paleo-Mesozoic tectonic evolution characteristics of Gucheng Lower uplift in Tarium Basin. J Jilin Univ (Earth Sci Ed) 48(2):545–555 (in Chinese with English abstract)

Liu YJ, Cao LM (1987) Introduction to element geochemistry. The Geological Publishing House, Beijing

Liu F, Liu ZJ, Liu R, Meng QT, Zhang J, Shi JZ, Du JF (2007) Geochemistry of oil shale from Jijuntun Formation of Eocene in Fushun Basin and its depositional environment. Global Geology 26(4):441–446 (in Chinese with English abstract). https://doi.org/10.1016/S1872-5813(08)60001-8

Liu ZB, Li HL, Qian YX, Sha XG, Ouyang ZZ, Yang GT (2012) Characteristics of Lower Paleozoic carbonate sediment and reservoir of Guchengxu uplift in Tazhong area. Chinese journal of geology 47(3):640–652 (in Chinese with English abstract)

Liu C, Zhang YJ, Li HH, Cao YH, Zhao YM, Zhang M, Zhou B (2017) Sequence stratigraphy classification and its geologic implications of Ordovician Yingshan Formation in Gucheng area, Tarim Basin. Journal of Northeast Petroleum University 41(1):82–96+122 (in Chinese with English abstract)

McLennan SM (1989) Rare earth elements in sedimentary rocks; influence of provenance and sedimentary processes. Rev Mineral Geochem 21(1):169–200

Mcmanus J, Berelson WM, Klinkhammer GP, Hammond DE, Holm C (2005) Authigenic uranium: Relationship to oxygen penetration depth and organic carbon rain. Geochim Cosmochim Acta 69(1): 95–108. https://doi.org/10.1016/j.gca.2004.06.023

Meyer EE, Quicksall AN, Landis JD, Link PK (2012) Trace and rare earth elemental investigation of a Sturtian cap carbonate, Pocatello, Idaho: evidence for ocean redox conditions before and during carbonate deposition. Precambrian Res 192-195:89–106. https://doi.org/10.1016/j.precamres.2011.09.015

Mongenot T, Tribovillard NP, Desprairies A, Lallier-Vergès E, Laggoun-Defarge F (1996) Trace elements as palaeoenvironmental markers in strongly mature hydrocarbon source rocks: the Cretaceous La Luna Formation of Venezuela. Sediment Geol 103(1-2):23–37. https://doi.org/10.1016/0037-0738(95)00078-X

Morford JL, Emerson S (1999) The geochemistry of redox sensitive trace metals in sediments. Geochim Cosmochim Acta 63(11-12):1735–1750. https://doi.org/10.1016/S0016-7037(99)00126-X

Murray RW, Brink MRBT, Gerlach DC, Iii GPR, Jones DL (1991) Rare earth, major, and trace elements in chert from the Franciscan Complex and Monterey Group, California: assessing REE sources to fine grained marine sediments. Geochim Cosmochim Acta 55(7): 1875–1895. https://doi.org/10.1016/0016-7037(91)90030-9

Qing HR, Veizer J (1994) Oxygen and carbon isotopic composition of Ordovician brachiopods: Implications for coeval seawater. Geochim Cosmochim Acta 58(20):4429–4442. https://doi.org/10.1016/0016-7037(94)90345-X

Rogers JJW, Adams JAS (1969) Abundances in rock forming minerals (I), uranium minerals (II). In: Wedepohl KH (ed) the Handbook of Geochemistry, Sect. 92-D. Springer, Berlin 92-D1-92- D2

Schroeder S, Grotzinger JP (2007) Evidence for anoxia at the Ediacaran-Cambrian boundary: the record of redox-sensitive trace elements and rare earth elements in Oman. J Geol Soc 164(1):175–187. https://doi.org/10.1144/0016-76492005-022

Sharp Z (2007) Principles of stable isotope geochemistry [M]. Houston, Pearson Education, pp 1–380

Shields G, Stille P (2001) Diagenetic constraints on the use of cerium anomalies as palaeoseawater redox proxies: an isotopic and REE study of Cambrian phosphorites. Chem Geol 175(1-2):29–48. https://doi.org/10.1016/S0009-2541(00)00362-4

Sun LG, Xie ZQ, Zhao JL (2000) The characteristics of sr/ba and b/ga ratios in lake sediments on the ardley peninsula, maritime Antarctic. Mar Geol Quat Geol 20(4):43–46 (in Chinese with English abstract)

Tang ZX, Cao ZC, Wang XW, Sha XG (2013) Reservoir characteristics and influencing factors in the inner Yingshan Formation in Guchengxu uplift, Tarim Basin. Lithologic reservoirs 25(4):47–52 (in Chinese with English abstract)

Tang LJ, Qiu HJ, Yun L (2014) Poly-phase reform-late-stage finalization composite tectonics and strategic area selection of oil and gas resources in Tarim Basin, NW China. J Jilin Univ (Earth Sci Ed) 44(1):1–14. https://doi.org/10.13278/j.cnki.jjuese.201401101

Taylor SR, Mclennan SM (1985) The continental crust: its composition and evolution. Blackwell Scientific Publications, Oxford, pp 1–312

Tissot B (1979) Effects on prolific petroleum source rocks and major coal deposits caused by sea-level changes. Nature 277(5696):463–465. https://doi.org/10.1038/277463a0

Tribovillard NP, Desprairies A, Lallier-Vergès E, Bertrand P, Moureau N, Ramdani A, Ramanampisoa L (1994) Geochemical study of organic-matter rich cycles from the Kimmeridge Clay Formation of Yorkshire (UK): productivity versus anoxia. Palaeogeogr Palaeoclimatol Palaeoecol 108(1-2):165–181. https://doi.org/10.1016/0031-0182(94)90028-0

Tribovillard N, Algeo TJ, Lyons T, Riboulleau A (2006) Trace metals as paleoredox and paleoproductivity proxies: an update. Chem Geol 232(1-2):12–32. https://doi.org/10.1016/j.chemgeo.2006.02.012

Veizer J (1983) Trace elements and isotopes in sedimentary carbonates. Rev Mineral Geochem 11(1):265–299. https://doi.org/10.1007/s11606-012-2065-x

Veizer J, Ala D, Azmy K, Strauss H (1999) $^{87}Sr/^{86}Sr$, $\delta^{13}C$ and $\delta^{18}O$ evolution of Phanerozoic seawater. Chem Geol 161:59–88. https://doi.org/10.1016/S0009-2541(99)00081-9

Wachter EA, Hayes JM (1985) Exchange of oxygen isotopes in carbon dioxide-phosporic acid systems. Chemical Geology: Isotope Geoscience Section 52(3-4):365–374. https://doi.org/10.1016/0168-9622(85)90046-6

Wang DR, Feng XJ (2002) Research on Carbon and Oxygen geochemistry of Lower Paleozoic in North China. Acta Geol Sin 76(3):400–408 (in Chinese with English abstract)

Wang HY, Fan TL, Zhao WS (2008) Study of the method for identification of carbonate logging sequence stratigraphy: a case study of the Ordovician in Kal area of Tazhong uplift, Tarim Basin. Earth Science Frontiers 15(2):51–58. https://doi.org/10.3321/j.issn:1005-2321.2008.02.007

Wang XM, Jiao YQ, Wu LQ, Rong H, Wang XM, Song J (2014a) Rare earth element geochemistry and fractionation in Jurassic coal from Dongsheng-Shenmu area, Ordos Basin. Fuel 136(15):233–239. https://doi.org/10.1016/j.fuel.2014.07.055

Wang G, Fan TL, Liu HL (2014b) Characteristics and Evolution of Ordovician Carbonate Platform Marginal Facies in Tazhong-Gucheng Area, Tarim Basin. Geoscience 28(5):995–1007 (in Chinese with English abstract)

Wang K, Liu W, Huang QY, Shi SY, Ma K, Liang DX (2015) Development Characteristics and Evolution of the Cambrian Sedimentary System in Tazhong and Gucheng Area,Tarim Basin. Geological Science and Technology Information 34(6):116–124 (in Chinese with English abstract)

Wang K, Hu SY, Hu ZY, Liu W, Huang QY, Shi SY, Ma K, Mei L (2016) Cambrian hydrothermal action in Gucheng area, Tarim Basin and its influences on reservoir development. Acta Pet Sin 37(4): 439–453. https://doi.org/10.7623/syxb201604003

Wei K, Li XB, Liu A, Li JT, Bai YS, Zhou P, Chen XH (2015) Trace element characteristics of carbonate rocks from the Ediacaran Doushantuo Formation of Xikou section, Cili County, Hunan Province and its palaeoenvironmental significance. J Palaeogeogr 17(3):297–308 (in Chinese with English abstract)

Wignall PB, Twitchett RJ (1996) Oceanic anoxia and the End Permian Mass Extinction. Science 272(5265):1155–1158. https://doi.org/10.1126/science.272.5265.1155

Wignall PB, Zonneveld JP, Newton RJ, Amor K, Sephton MA, Hartley S (2007) The end Triassic massextinction record of Williston Lake, British Columbia. Palaeogeogr Palaeoclimatol Palaeoecol 253(3-4): 385–406. https://doi.org/10.1016/j.palaeo.2007.06.020

Wright J, Schrader H, Holser WT (1987) Paleoredox variations in ancient oceans recorded by rare earth elements in fossil apatite. Geochim

Cosmochim Acta 51(3):631–644. https://doi.org/10.1016/0016-7037(87)90075-5

Wu SB (2001) Sedimentary Facies and Depositional Model of Wulabo Formation, Upper Permian Series in Bogeda Piedmont Depression, Junggar Basin. Acta Sedimentol Sin 19(3):333–339 (in Chinese with English abstract)

Xu LH, Chen JF, Li L, Ma GY, Liu YD (2009) Carbon, oxygen isotope and trace element characteristics of carbonate rocks in Changxing-Feixianguan Formation of Pu-guang gas pool and its palaeoenvironment significance. Acta Geosci Sin 30(1):103–110 (in Chinese with English abstract)

Yan L, Li M, Pan WQ (2014) Distribution characteristics of Permian igneous rock in Tarim Basin-based on the high-precision aeromagnetic data. Prog Geophys 29(4):1843–1848

Yang HJ, Li Y, Liu S, Li XS, Chen JS, Wang ZY, Dai ZY (2000) Classification and correlation of Middle-Upper Ordovician in Tazhong area and its key understanding. Xinjiang Petroleum Geology 21(3):208–212 (in Chinese with English abstract)

Yu BS, Dong HL, Widom E, Chen JQ, Lin CS (2009) Geochemistry of Basal Cambrian Black Shales And Cherts From The Northern Tarim Basin, Northwest China: Implications For Depositional Setting And Tectonic History. J Asian Earth Sci 34(3):418–436. https://doi.org/10.1016/j.jseaes.2008.07.003

Yu XF, Tang HS, Han ZZ, Li CY (2010) Geological characteristic and origin of rare earth elements deposits related with alkaline rock in the Chishan-Longbaoshan area, Shandong province. Acta Geol Sin 84(3):407–417

Yu BS, Lin CS, Fan TL, Wang LD, Gao ZQ, Zhang C (2011) Sedimentary response to geodynamic reversion in Tarim Basin during Cambrian and Ordovician and its significance to reservoir development. Earth Science Frontiers 18(3):221–232

Zhang XL (1985) Relationship between Carbon and Oxygen stable isotope in carbonate rocks and paleosalinity and paleotenperature of seawater. Acta Sedimentol Sin 3(4):17–30 (in Chinese)

Zhang SB, Huang ZB, Zhu HC (2004) Phanerozoic strata in the coverage areas of the Tarim Basin. Petroleum Industry Press, Beijing, pp 1–300

Zhang QY, Jia JD, Jin JQ (2007) Characteristics of Cambrian-Ordovician sedimentary facies in Tadong region and its sedimentary model. Nat Gas Geosci 18(2):229–234

Zhang GY, Liu W, Zhang L, Yu BS, Li HH, Zhang BM, Wang LD (2015) Cambrian-Ordovician prototypic basin, paleogeography and petroleum of Tarim Craton. Earth Science Frontiers 22(3):269–276 (in Chinese with English abstract). https://doi.org/10.13745/j.esf.2015.03.023

Zhao ZJ (2015) Indicators of global sea-level change and research methods of marine tectonic sequences: take Ordovician of Tarim Basin as an example. Acta Pet Sin 36(3):262–273

Zhao M, Gan HJ, Yue Y, Jiang H, Lin ZL, Fang XX (2009) Characteristics of Ordovician carbonate reservoir in the western plunge of Gucheng uplift, Tarim basin. Geol China 36(1):93–100 (in Chinese with English abstract)

Zheng XP, Zhou JG, Wu XN (2004) High-frequency sequence quantitative analysis technology of carbonate rock and its application. China Petroleum Exploration 9(5):26–30. https://doi.org/10.3969/j.issn.1672-7703.2004.05.005

Zheng JF, Shen AJ, Mo NY, Liu YF (2010) Genesis and feature identification of Cambrian-Lower Ordovician dolostone in Tarim Basin. Marine Original Petroleum Geology 15(1):6–14 (in Chinese with English abstract)

Zheng YL, Ma ZQ, Wang BC, Yuan GL, Qin JX (2015) Geochemistry characteristics and sedimentary environment of oil shale from the Eocene Bahuli Formation in Liushuhe Basin, Heilongjiang Province. J Palaeogeogr 17(5):689–698 (in Chinese with English abstract)

Zhou XX, Lü XX, Zhu GY, Cao YH, Yan L, Zhang ZY (2019) Origin and formation of deep strata gas from Gucheng-Shunnan Block of Tarim Basin, NW China. J Pet Sci Eng 177:361–373. https://doi.org/10.1016/j.petrol.2019.02.059

Zhu XM (2000) Sequence Stratigraphy. China University of Petroleum Press, pp 1–205

Zhu DY, Jin ZJ, Hu WX (2010) Hydrothermal recrystallization of the lower Ordovician dolomite and its significance to reservoir in north Tarim Basin. Sci China Earth Sci 53(3):368–381. https://doi.org/10.1111/j.1365-313X.2007.03127.x